Computers and Geotechnics 68 (2015) 91–108

Contents lists available at ScienceDirect

Computers and Geotechnics

journal homepage: www.elsevier.com/locate/compgeo

Research Paper

The simulation and discretisation of random fields for probabilistic finite element analysis of soils using meshes of arbitrary triangular elements

David K.E. Green [a,*], Kurt Douglas [a], Garry Mostyn [b]

[a] School of Civil & Environmental Engineering, University of New South Wales, Sydney, NSW 2052, Australia
[b] Pells Sullivan Meynink, Sydney, NSW 2113, Australia

ARTICLE INFO

Article history:
Received 23 October 2014
Received in revised form 1 April 2015
Accepted 7 April 2015
Available online 20 April 2015

Keywords:
Monte Carlo Simulation
Random fields
Local averaging
Gaussian quadrature
Cholesky decomposition
Slope stability

ABSTRACT

This paper presents a new methodology to discretise random fields for reliability assessment by the Random Finite Element Method. The methodology maps a random field to an arbitrary triangular finite element mesh by local averaging. Derivations for the variance reduction and covariance between local averages of triangular areas using numeric integration are presented. The new methodology is compared against a published reliability assessment of a drained slope. The results matched expectations that not accounting for spatial variability will, in the case analysed, significantly underestimate reliability. A method to generate random fields using a form of Cholesky decomposition appropriate even for singular covariance matrices is presented and analysed. Finally, the derivations for the discretisation of random fields onto triangular meshes are presented for three dimensional tetrahedral elements.

© 2015 Elsevier Ltd. All rights reserved.

1. Introduction

Soils exhibit significant variations in their measured material property parameters even within apparently homogeneous layers [14]. The typical approach to the modelling of soil property variability in geotechnical engineering involves either the assumption of homogeneity or the application of simple probabilistic models. These models do not adequately quantify the risks of a given design [32]. In this paper, a new development in advanced probabilistic modelling of soils using random fields is presented.

Reliability of a design can be defined in a probabilistic sense as the chance that a structure is able to withstand the loads to which it will be subjected. The majority of simple numerical modelling techniques underestimate the reliability of geotechnical designs provided the factor of safety is greater than one [33]. Excessive conservatism may lead to decisions where either safe designs are considered to have unacceptable levels of risk or, alternatively, over time the perception of what constitutes acceptable risk may become distorted in practice. The cost of overdone conservatism, particularly in long design life civil projects, is economically wasteful and may even render an otherwise sound design financially unviable [32,27]. Of course, a lack of conservatism could result in disaster. When comparing strengths and weaknesses of different numerical analysis models, the fundamental issue is the manner in which a model quantifies risk. Simple analysis methods, such as deterministic limit equilibrium analyses, rely almost entirely on practitioner judgement and qualitative assessment in order to assess risk. Probabilistic methods provide a means to assess the reliability of a given design in terms of acceptable risk. This paper focusses specifically on modelling the variability of soils.

Soil property variability can be modelled as being composed of two components, point and spatial variability. Point variability describes the variations in a measured property recorded independent of position (e.g. direct shear tests carried out on multiple samples taken from across a site) typically modelled with a probability density function. Spatial variability describes how the value of some parameter varies with distance between points and can be defined by a correlation function. The mathematical construct that combines point and spatial variability is termed a random field. Random field models of soil parameters have become increasingly common as the reliability of a design is known to be sensitive to the effects of spatial variability [13,28].

Several methods exist for the computation of the reliability of a given design. One of the most promising techniques available is the Random Finite Element Method (RFEM) [14]. In this methodology, a Monte Carlo Simulation is undertaken in which a random field is repeatedly simulated, mapped onto a finite element mesh and then solved deterministically by finite elements for failure/non-failure. The key advantage of this approach is that the full system

* Corresponding author. Tel.: +61 2 9385 5033.
E-mail address: d.k.green@unsw.edu.au (D.K.E. Green).

http://dx.doi.org/10.1016/j.compgeo.2015.04.004
0266-352X/© 2015 Elsevier Ltd. All rights reserved.

reliability is computed, as opposed to methods which only analyse a single failure mechanism. Assuming enough simulation runs are completed, the stresses within the finite element model are able to seek out the probabilistic critical failure mechanism.

RFEM makes use of local averaging theory in order to map a random field over an infinite set of points to a discrete finite element mesh [14]. The use of local averaging for random field discretisation is well supported [14,43,44]. A disadvantage with RFEM, as it has been implemented in previous studies, is that only rectangular finite element meshes have been used. The local average subdivision (LAS) algorithm, used heavily in [14], would be difficult to carry out over arbitrarily oriented elements. Regular, rectangular meshes can be impractical. Arbitrarily oriented triangular elements may be required to mesh a problem domain when complicated geometry is present. In this paper, a methodology for the simulation and discretisation of random fields, including the effects of local averaging, for finite element meshes of triangular elements is presented. This methodology was implemented in a computer program, NIRFS, developed by the authors.

In order to test the validity of the random field simulation methodology presented, results from NIRFS were compared against a published reliability assessment of a slope stability problem. Many studies have focussed on probabilistic slope stability analysis, [14] presents a list of 21 significant references. Ji et al. in [27] present the results of a reliability assessment of a simple drained slope based on a limit equilibrium approach where the material properties along the critical failure surface are modelled using random fields. A comparison between NIRFS and the analysis in [27] is presented in Section 4 of this paper.

2. Computing the correlation structure of locally averaged random fields

2.1. Monte Carlo Simulation by the Random Finite Element Method

The Random Finite Element Method [14,20] can be used to compute the system reliability of design. RFEM is a Monte Carlo Simulation process. For each discrete simulation, a random field is simulated, mapped onto a finite element mesh using local averaging and then solved deterministically by finite elements for failure/non-failure. The probability of failure can then be computed as the proportion of failed simulations to the total number of simulations. A flowchart of this procedure is presented in Fig. 1.

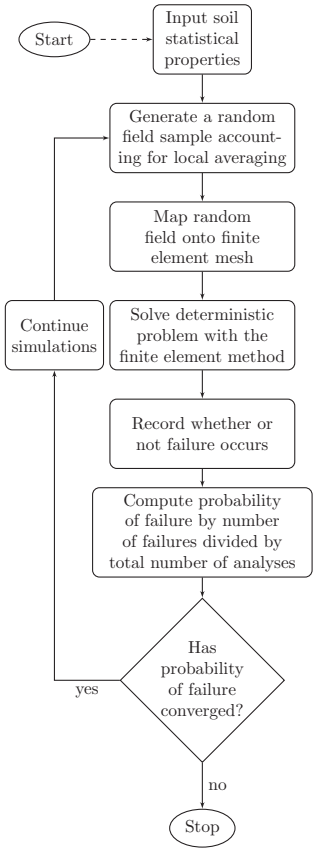

Fig. 1. Flowchart of RFEM simulation methodology.

2.2. Random field representation

Extensive formal definitions of random fields can be found in [14,43,1]. Gaussian random fields are commonly used as they are completely specified by their first two moments, the mean and covariance of the random field. A Gaussian random field is represented by an infinite multivariate Gaussian distribution between all points, $(x_1, x_2, \ldots, x_k)$, in some spatial domain. Mathematically, this is given as:

$$f_{x_1 x_2 \ldots x_k}(x_1, x_2, \ldots, x_k) = \frac{1}{(2\pi)^{\frac{k}{2}}|\mathbf{C}|^{\frac{1}{2}}} \exp\left(-\frac{(x-\mu)^T \mathbf{C}^{-1}(x-\mu)}{2}\right) \quad (1)$$

where μ is the mean vector of the random field, and $\mathbf{C}$ is the covariance matrix with entries given by the covariance between points i and j equal to $C_{ij}(\tau_{ij})$ where τ_{ij} is either the separation distance or a lag-vector between points i and j. If τ_{ij} is the distance between points i and j, the field is isotropic. The covariance function $C_{ij}(\tau_{ij})$ can be expressed in terms of an underlying correlation function, $\rho_{ij}(\tau_{ij})$, and the standard deviations of the Gaussian distributions at each point, σ_i and σ_j, such that $C_{ij}(\tau_{ij}) = \sigma_i \sigma_j \rho_{ij}(\tau_{ij})$.

The covariance function need not be isotropic. C_{ij} can be found using the directional components of τ_{ij} if this quantity is computed as a vector with magnitude equal to the distance between i and j. A random field can be considered weakly homogeneous if the mean and standard deviation are invariant across the field [34]. In this paper, only fields of this type are considered.

2.3. Local averaging of random fields for field discretisation

To simulate random fields, it is necessary to discretise the infinite set of points that the field represents mathematically into a representation suitable for use with computers. Several methods exist for the discretisation of a random field, Sudret and Der Kiureghian [40] contains an extensive review. In this paper, a local averaging, see [44], approach is adopted in order to discretise a random field onto a triangular finite element mesh. The modelling of engineering property parameters by local averages is discussed at length in Fenton and Griffiths [14]. The argument for this can be summarised by considering that most engineering property parameters used for modelling macro-scale problems are poorly defined for an infinitesimally small domain. Modulus and porosity are examples of this.

In order to discretise a random field by local averaging two formulations must be known, namely the variance reduction function and the covariance between local averages. Locally averaging over some finite element reduces the variance of a discretised random field when compared to the original infinite joint distribution. If this filtering process is not applied, the correlation structure of the random field will not be correctly modelled on the discretised field. Analogous to techniques common in digital signal processing, small scale fluctuations much smaller than the scale of the discretisation must be filtered out. This ensures that, when sampling

from a random field, the probability of obtaining a particular sample is the same in both the infinite Gaussian distribution and the discretised approximation. In particular, without recourse to local averaging, it can be impossible to gain accurate probability of failure estimates. Demonstrations of these effects are shown for analysis of sheet pile walls in walls [7] and shallow foundations in [36].

The variance reduction function is used to calculate this effect. If the covariance between local averages is able to be computed, a locally averaged representation of a random field can be simulated such that the effect of the size of the finite elements in the mesh is incorporated accurately [44]. Using this approach, the entries of the covariance matrix C_{ij} are given by the covariance between the local averages of elements i and j. This is in contrast to the midpoint method in which values for the random field are found only at the midpoint of each finite element. The midpoint method is known to overestimate the variance of the discretised random field [34].

The following operators are used in this paper: $E[x]$: Expectation of x, $Var[x]$: Variance of x, $Cov[x,y]$: Covariance of x and y.

2.4. Derivation of variance reduction function for two-dimensional areas

For a two-dimensional random field, $X(x,y)$, the locally averaged random field, $X_\Omega(x,y)$, over some area, Ω, can be given as:

$$X_\Omega(x,y) = \frac{1}{\Omega}\iint_\Omega X(x,y)dydx \tag{2}$$

The following property of variance from Theorem 2.4 in [29] is useful:

$$Var[x] = E[x - E[x]]^2$$
$$Var[x] = E[x^2] - E[x]^2$$

Also, the expectation of the local average, $E[X_\Omega]$, is equal to the mean of the random field (for a stationary random field) as:

$$E[X_\Omega] = E\left[\frac{1}{\Omega}\iint_\Omega X(x,y)dydx\right]$$
$$E[X_\Omega] = \frac{1}{\Omega}\iint_\Omega E[X(x,y)]dydx$$
$$E[X_\Omega] = E[X(x,y)]$$

Let μ be the mean of the random field so $E[X(x,y)] = \mu$. Then variance reduction γ over a two-dimensional region, Ω of area A_Ω, can be derived by finding the variance of the locally averaged area in terms of the variance of the original random field. Then, for a non-zero mean random field:

$$Var[X_\Omega] = E\left[\frac{1}{A_\Omega^2}\left(\iint_\Omega X(p_1)d\Omega\right)\left(\iint_\Omega X(p_2)d\Omega\right)\right] - \mu^2 \tag{3}$$

From this point, the term μ^2 can be removed and, to simplify the algebra, the variance reduction found in terms of a zero mean random field:

$$Var[X_\Omega] = E\left[\tfrac{1}{A_\Omega^2}\left(\iint_\Omega X(p_1)d\Omega\right)\left(\iint_\Omega X(p_2)d\Omega\right)\right]$$
$$Var[X_\Omega] = \tfrac{1}{A_\Omega^2}\iint_\Omega\iint_\Omega E[X(p_1)X(p_2)]d\Omega d\Omega$$
$$Var[X_\Omega] = \tfrac{1}{A_\Omega^2}\iint_\Omega\iint_\Omega Cov[X(p_1),X(p_2)]d\Omega d\Omega$$
$$Var[X_\Omega] = \tfrac{1}{A_\Omega^2}\iint_\Omega\iint_\Omega C_X(p_2-p_1)d\Omega d\Omega$$
$$Var[X_\Omega] = \tfrac{\sigma^2}{A_\Omega^2}\iint_\Omega\iint_\Omega \rho_X(p_2-p_1)d\Omega d\Omega$$

This derivation yields, for a zero mean random field:

$$Var[X_\Omega] = \sigma^2\gamma \tag{4}$$

Then:

$$\gamma = \frac{Var[X_\Omega]}{\sigma^2}$$
$$\gamma = \frac{1}{A_\Omega^2}\iint_\Omega\iint_\Omega \rho_X(p_2-p_1)d\Omega d\Omega \tag{5}$$

For a random field with expectation μ:

$$\gamma = \frac{1}{A_\Omega^2}\iint_\Omega\iint_\Omega \rho_X(p_2-p_1)d\Omega d\Omega - \frac{\mu^2}{\sigma^2}$$

The derivation of variance reduction for a general two-dimensional area can be found in [14,43]. The closed form solution of the integral in Eq. (5) is highly dependent on the limits of the area integrals and the form of the correlation function ρ_X. Closed form solutions are known for various classes of covariance functions for rectangular areas [43].

2.5. Derivation of variance reduction for triangular areas by Gaussian quadrature

Given the forms of common covariance functions, it is simple to generate integrals using Eq. (5) that cannot be solved. To simplify the matter, it is far easier and more general to perform numerical integration via Gaussian quadrature. Using this method, an integral is approximated by determining the value of the function at predetermined points then adding the weighted sum of the function at these points. This particular method of numerical integration has the advantage of being simple to implement in computer code.

The form of Gaussian quadrature adopted here is that given in [10] which gives the integration of a function over a triangular region, Ω of area A_Ω as:

$$\iint_\Omega f(p)d\Omega \approx A_\Omega\sum_{i=1}^{N} w_i f(\lambda_{1i},\lambda_{2i},\lambda_{3i}) \tag{6}$$

where p is a coordinate vector in (x,y), N is the adopted degree of precision of the solution, $(\lambda_{1i},\lambda_{2i},\lambda_{3i})$ are the i-th sampling points (expressed in homogeneous barycentric coordinates) and w_i is the quadrature weight associated with the i-th sampling point. Homogeneous barycentric coordinates (Fig. 2) are expressed in terms of the weighted sum of the distances from the vertex coordinates such that given a triangle with vertices $\mathbf{r}$:

$$\mathbf{r} = \begin{pmatrix} r_1 \\ r_2 \\ r_3 \end{pmatrix} = \begin{pmatrix} x_1, y_1 \\ x_2, y_2 \\ x_3, y_3 \end{pmatrix}$$

Any point within this triangle can be represented as the weighted sum of these vertices: $\mathbf{r} = \lambda_1 r_1 + \lambda_2 r_2 + \lambda_3 r_3$ subject to the constraint that $\lambda_1 + \lambda_2 + \lambda_3 = 1$. From [47], barycentric coordinates can then be converted back to triangular coordinates by:

$$x(\lambda_1,\lambda_2) = \lambda_1(x_1 - x_3) + \lambda_2(x_2 - x_3) + x_3 \tag{7}$$
$$y(\lambda_1,\lambda_2) = \lambda_1(y_1 - y_3) + \lambda_2(y_2 - y_3) + y_3 \tag{8}$$

Combining Eqs. (5) and (6) the integration of the covariance function over an arbitrary triangle, for a zero mean random field, can be simplified to:

$$Var[X_\Omega] \approx \frac{\sigma^2}{A_\Omega^2}A_\Omega^2\sum_{i=1}^{N}\sum_{j=1}^{N} w_i w_j \rho_X(\lambda_{1j}-\lambda_{1i},\lambda_{2j}-\lambda_{2i},\lambda_{3j}-\lambda_{3i})$$
$$Var[X_\Omega] \approx \sigma^2\sum_{i=1}^{N}\sum_{j=1}^{N} w_i w_j \rho_X(\lambda_{1j}-\lambda_{1i},\lambda_{2j}-\lambda_{2i},\lambda_{3j}-\lambda_{3i})$$

For notational convenience, define:

$$\lambda_{m,ji} := \lambda_{mj} - \lambda_{mi} \tag{9}$$

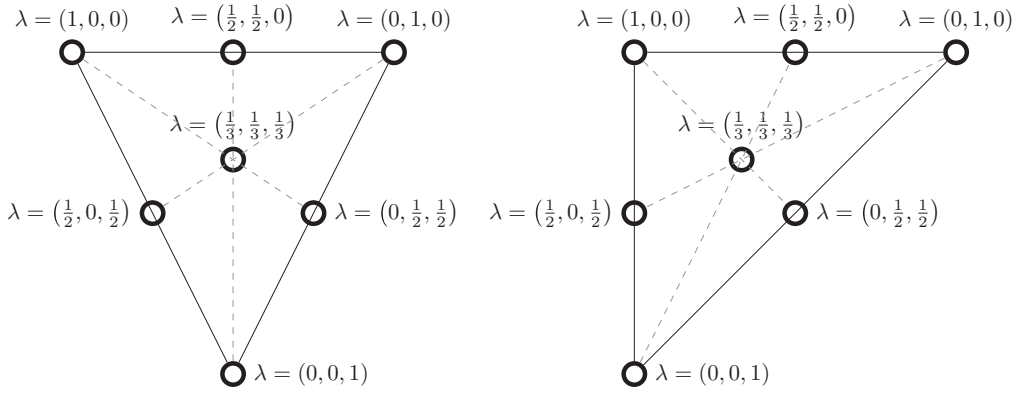

Fig. 2. Homogeneous barycentric coordinates $(\lambda_1, \lambda_2, \lambda_3)$ on equilateral and right angle triangles.

where m, i and j are indexing integers so that the computation for variance above can be written as:

$$Var[X_\Omega] \approx \sigma^2 \sum_{i=1}^{N}\sum_{j=1}^{N} w_i w_j \rho_X(\lambda_{1,ji}, \lambda_{2,ji}, \lambda_{3,ji}) \tag{10}$$

Given Eq. (4), the formula for the variance reduction over a triangular area can be computed by:

$$\gamma \approx \sum_{i=1}^{N}\sum_{j=1}^{N} w_i w_j \rho_X(\lambda_{1,ji}, \lambda_{2,ji}, \lambda_{3,ji}) \tag{11}$$

If the mean is non-zero, the constant term (for a stationary random field) μ^2/σ^2 can be subtracted so:

$$\gamma \approx \sum_{i=1}^{N}\sum_{j=1}^{N} w_i w_j \rho_X(\lambda_{1,ji}, \lambda_{2,ji}, \lambda_{3,ji}) - \frac{\mu^2}{\sigma^2}$$

2.6. Covariance between local averages of triangular elements by Gaussian quadrature

In order to simulate a locally averaged random field, it is necessary to compute the covariance between local averages rather than the covariance between points within the field. This ensures that the effect of element size is captured. Given a pair of two dimensional regions, Ω and Ψ of area A_Ω and A_Ψ, the value of the random field is given by $X_\Omega(x,y)$ and $X_\Psi(x,y)$ respectively. Recall from Section 2.4 that, for a stationary random field, $E[X_\Omega] = \mu$ where μ is the mean of the random field.

With local averages expressed as in Eq. (2) the covariance between the local averages of $X_\Omega(x,y)$ and $X_\Psi(x,y)$ can be found by:

$$Cov[X_\Omega, X_\Psi] = Cov\left[\frac{1}{A_\Omega}\iint_\Omega X(p_\Omega)d\Omega - \mu, \frac{1}{A_\Psi}\iint_\Psi X(p_\Psi)d\Psi - \mu\right]$$
$$Cov[X_\Omega, X_\Psi] = Cov\left[\frac{1}{A_\Omega}\iint_\Omega X(p_\Omega)d\Omega, \frac{1}{A_\Psi}\iint_\Psi X(p_\Psi)d\Psi\right] - \mu^2$$

Then, for a zero mean random field the μ^2 term can be ignored for convenience and:

$$Cov[X_\Omega, X_\Psi] = Cov\left[\frac{1}{A_\Omega}\iint_\Omega X(p_\Omega)d\Omega, \frac{1}{A_\Psi}\iint_\Psi X(p_\Psi)d\Psi,\right]$$
$$Cov[X_\Omega, X_\Psi] = \frac{1}{A_\Omega A_\Psi}\iint_\Omega\iint_\Psi Cov[X(p_\Omega), X(p_\Psi)]d\Psi d\Omega$$
$$Cov[X_\Omega, X_\Psi] = \frac{1}{A_\Omega A_\Psi}\iint_\Omega\iint_\Psi C_X(p_\Psi - p_\Omega)d\Psi d\Omega$$
$$Cov[X_\Omega, X_\Psi] = \frac{\sigma_\Omega \sigma_\Psi}{A_\Omega A_\Psi}\iint_\Omega\iint_\Psi \rho_X(p_\Psi - p_\Omega)d\Psi d\Omega \tag{12}$$

where σ_Ω and σ_Ψ are the reduced standard deviations for the local averages $X_\Omega(x,y)$ and $X_\Psi(x,y)$ computed using Eqs. (4) and (11). The above general derivation can be found in [14]. For a non-zero random field, Eq. (12) becomes:

$$Cov[X_\Omega, X_\Psi] = \frac{\sigma_\Omega \sigma_\Psi}{A_\Omega A_\Psi}\iint_\Omega\iint_\Psi \rho_X(p_\Psi - p_\Omega)d\Psi d\Omega - \mu^2$$

Given the form of numerical integration over triangular areas given in Eq. (6) and the formulation for the covariance between two-dimensional areas in Eq. (12) the covariance between two triangular areas can then be expressed as:

$$Cov[X_\Omega, X_\Psi] \approx \sigma_\Omega \sigma_\Psi \sum_{i=1}^{N}\sum_{j=1}^{N} w_i w_j \rho_X(\lambda_{1,ji}, \lambda_{2,ji}, \lambda_{3,ji}) - \mu^2 \tag{13}$$

Note that this form is similar to that derived for variance reduction over triangular areas. The difference is that the sampling points λ_i and λ_j are taken from the local averages $X_\Omega(x,y)$ and $X_\Psi(x,y)$ respectively, rather than all sampling points being taken within the same triangular area. The similarity is to be expected as the variance is simply equal to the covariance of a region with itself.

2.7. Variance and covariance for tetrahedral elements by Gaussian quadrature

The equations derived for triangular elements can be generalised to three dimensional (tetrahedral) and higher dimensional analogues of triangles (simplicial elements) as these shapes also permit a simple description in terms of barycentric coordinates. While not used for the analyses presented within, the three-dimensional equations for variance reduction and covariance are presented for completeness. As the algebra is simpler for a zero-mean random field, all results in this section assume $\mu = 0$. The inclusion of $\mu \neq 0$ terms in the following equations is analogous to the two-dimensional case and is a simple exercise.

The form of Gaussian quadrature adopted here is modified, notationally only, from that given in [46], in which the quadrature weights can also be found. The integration of a function over a tetrahedral volume, V, can be approximated as:

$$\iiint_V f(p)dV \approx V\sum_{i=1}^{N} w_i f(\lambda_{1i}, \lambda_{2i}, \lambda_{3i}, \lambda_{4i}) \tag{14}$$

The variance reduction within a tetrahedral volume, Ω, of volume V_Ω can be derived in the same manner as that for Eq. (4). The variance reduction is:

$$\gamma = \frac{Var[X_\Omega]}{\sigma^2}$$
$$\gamma = \frac{1}{V_\Omega^2}\iiint_\Omega \iiint_\Omega \rho_X(p_2 - p_1)d\Omega d\Omega \tag{15}$$

The variance reduction across Ω can be approximated using the quadrature relationship in Eq. (14). Using the same notational convention as that shown in Eq. (9):

$$\gamma \approx \sum_{i=1}^{N}\sum_{j=1}^{N} w_i w_j \rho_X(\lambda_{1,ji}, \lambda_{2,ji}, \lambda_{3,ji}, \lambda_{4,ji})$$

The covariance between two tetrahedral volumes, Ω and Ψ of volume V_Ω and V_Ψ respectively, can be found using their local averages, X_Ω and X_Ψ by the same procedure as that shown to derive Eq. (12). Following this derivation for tetrahedral volumes instead of triangular areas yields:

$$Cov[X_\Omega, X_\Psi] = \frac{\sigma_\Omega \sigma_\Psi}{V_\Omega V_\Psi}\iiint_\Omega \iiint_\Psi \rho_X(p_\Psi - p_\Omega)d\Psi d\Omega \tag{16}$$

This can, again, be approximated by quadrature:

$$Cov[X_\Omega, X_\Psi] \approx \sigma_\Omega \sigma_\Psi \sum_{i=1}^{N}\sum_{j=1}^{N} w_i w_j \rho_X(\lambda_{1,ji}, \lambda_{2,ji}, \lambda_{3,ji}, \lambda_{4,ji}) \tag{17}$$

3. Random fields simulation discretised by arbitrarily oriented triangular finite element meshes

3.1. Random field simulation and triangular mesh discretisation

To carry out a RFEM analysis, samples from the random field used to describe the input parameters must be generated. For the simulations presented in Section 4, a random field generator based on decomposition of the covariance matrix was used. Covariance matrix decomposition was found to be the most appropriate method to generate random fields discretised by arbitrary meshes of triangular elements. In this section, a justification for the use of such a method is presented in terms of computational complexity, numerical precision and issues specific to arbitrary triangular meshes. Methods for resolving numerical stability problems that may arise with matrix decomposition random field generators are also discussed.

While several methods exist for the simulation of random fields, as detailed in [14], the majority of these methods are only appropriate for generating random field samples discretised by rectangular, or almost rectangular, grids. For example, LAS and the fast Fourier transform (FFT) algorithms generate random fields over regular grids. Complicated mesh geometry can destroy the required form of the random field correlation structure that make LAS and FFT generators efficient and would be difficult to apply to arbitrary triangular meshes. One possible technique to do so would be to generate a random field over a sufficiently fine regular grid and then map this using local averaging to the triangular mesh. Such a method would prevent the correlation structure from being discretised accurately unless a very fine grid was used. It may also be possible to use some curvilinear mapping of the triangular mesh to some regular rectangular grid. FFT or LAS could then be applied to this rectangular grid and then an inverse transform applied. Such a transformation from the triangular space to the rectangular space and its inverse is likely complicated and is clearly not bijective. Using the results derived in Section 2, it should be possible to derive a triangular version of LAS. As such a method does not yet exist, it has not been used for the results in this paper.

Alternatively, the turning bands method (TBM), detailed in [14], is suitable for handling arbitrary geometry. TBM involves generating a series of one dimensional random field samples along arbitrarily oriented lines and building the desired two or three dimensional random field sample from these line processes. At each point in the discrete output field, a weighted contribution from each one dimensional random field is added based on the perpendicular distance of the point to the line. However, when the correlation function is anisotropic, TBM can be difficult to use as discussed in [13]. The precision of the method is dependent on both the one dimensional random field generator and the number of individual lines used. If an insufficient number of lines are used, streaked patterns emerge that may cause unrealistic preferential stress or flow paths during finite element analysis [13,14]. Finally, difficulties also arise in deciding how to discretise the one dimensional line processes and the interaction of this discretisation with a triangular mesh. If a very dense discretisation is used to minimise errors caused by the generation of the line process, any potential efficiency gains from using a graded mesh will be lost. Alternatively, some discretisation that is calculated based on the relative orientation and size of triangular elements to the current line process could be calculated although this calculation would be, again, necessarily constrained by the smallest elements in the mesh and difficult to calculate. Once the discretisation of the line processes becomes fine enough, then essentially one is generating a random field over a fine grid and then mapping this to a triangular finite element mesh. The problems with this are discussed above.

Methods based on decomposition of the covariance matrix are able to generate random fields with an accurate correlation structure over a triangular mesh. The structure of the mesh is directly incorporated into the simulation, without any need for remapping the random field to the mesh. Matrix decomposition methods include the Cholesky, LDL and Modal decompositions [18,29,14]. Very roughly, these methods extract a set of basis vectors from the covariance matrix, such that a set of uncorrelated random samples can be transformed into a correctly correlated sample from the random field. Pairs of basis vectors can be considered as representing an ellipse. The correlation between a pair of basis vectors is effectively represented by the orientation of this ellipse. Techniques for random field generation by covariance matrix decomposition and potential pitfalls are discussed in the remainder of this section.

3.2. Random field simulation by matrix decomposition

Although not popular in random field simulation for geotechnics [13], the matrix decomposition, in particular the Cholesky decomposition, is widely used in other fields to generate samples from multivariate normal distributions [29]. The theoretical properties of matrix decomposition techniques in terms of infinite precision arithmetic are first addressed. Any practical implementation will be limited to some finite precision approximate calculation. The implications of finite precision floating point arithmetic on the decomposition of the covariance matrix are discussion in Section 3.4.

All matrix decomposition random field generators first start by forming the covariance matrix **C**. For a locally averaged random field, the entries of **C** are the covariances between local averages. For n elements in a finite element mesh, **C** is of size $n \times n$. The entries of **C** are given by $C_{i,j}$ equal to $Cov[X_i, X_j]$ which is computed as in Eq. (13). The covariance matrix is always symmetric [14] and positive semi-definite [24]. These properties will be relevant for the rest of this section.

3.2.1. Eigenvalues and eigenvectors of the covariance matrix

To facilitate discussion of random field sampling by covariance matrix decomposition, it is useful to first explore the eigenvalues and eigenvectors of the covariance matrix. By Theorem 8.1.1 in

[18], given a symmetric matrix $\mathbf{C}$ of size $n \times n$, there exists an orthogonal matrix $\mathbf{Q}$ (that is, all column vectors are orthogonal) such that:

$$\mathbf{Q}^T\mathbf{C}\mathbf{Q} = \mathbf{\Lambda} = \text{diag}(\lambda_1, \ldots, \lambda_n) \tag{18}$$

where T denotes the matrix transpose. Also, $\text{diag}(\lambda_1, \ldots, \lambda_n)$ refers to a diagonal matrix, a matrix with zero in all entries except along the main diagonal which instead has λ_1 in the first row, λ_2 in the second row and so on. Eq. (18) can be reorganised to the form:

$$\mathbf{C}\mathbf{Q} = \mathbf{Q}\mathbf{\Lambda} \tag{19}$$

Presented in this way, $\mathbf{Q}$ is more clearly the matrix whose columns are the eigenvectors of $\mathbf{C}$ and $\mathbf{\Lambda}$ stores the corresponding eigenvalues along the main diagonal. As the eigenvalues can always be reordered into any permutation, let λ_i denote the i-th largest eigenvalue of $\mathbf{C}$. As $\mathbf{C}$ is positive semi-definite, all of the eigenvalues, $\lambda_1, \ldots, \lambda_n$ are greater than or equal to zero (Theorem 4.1.10 in [24]). Then, if there are k non-zero eigenvalues:

$$0 = \lambda_n = \cdots = \lambda_{k+1} < \lambda_k \leqslant \cdots \leqslant \lambda_1 \tag{20}$$

By Theorem 4.1.10 of [24], if all of the eigenvalues are strictly greater than zero, that is $k = n$ in Eq. (20), then $\mathbf{C}$ is positive definite (rather than semi-definite). By Observation 1.1.7 in [24], a matrix is singular if and only if 0 is in the set of eigenvalues. By Conditions 3.7.5 and 3.7.6 (and the proof of their equivalence) in [31], if an $n \times n$ matrix is non-singular then the rank (number of linearly independent columns) of the matrix is n. So then a symmetric positive definite matrix of size $n \times n$ is non-singular and has full rank (all columns are linearly independent).

Conversely, the rank-nullity theorem states that for an $n \times n$ matrix $\mathbf{C}$:

$$n = \text{rank}(\mathbf{C}) + \dim(\text{nullspace}(\mathbf{C})) \tag{21}$$

where $\text{nullspace}(\mathbf{C})$ is defined by $\mathbf{C}x = 0$ where x is a vector of length n. But if zero is in the set of eigenvalues, the matrix is singular and so $\text{rank}(\mathbf{C}) < n$ and the columns of $\mathbf{C}$ have linear dependencies. From [16]:

$$\dim(\text{nullspace}(\mathbf{C})) = k \tag{22}$$

where k is the number of zero eigenvalues as in Eq. (20).

Combining Eqs. (21) and (22) the results concerning singularity and positive definiteness can be summarised. Let k be the number of eigenvalues equal to 0 of $\mathbf{C}$. If k is greater than zero, then $\mathbf{C}$ is singular and positive semi-definite. If $k = 0$, then $\mathbf{C}$ is positive definite. Additionally, the number of linearly dependent columns of $\mathbf{C}$ is equal to k so:

$$\text{rank}(\mathbf{C}) = n - k \tag{23}$$

It is useful to provide a bound on the eigenvalues of $\mathbf{C}$ to facilitate the rounding error analysis in Section 3.4. As the effect of variance reduction on σ only reduces the order of magnitude of σ, the effect of γ on σ can be excluded to simplify the eigenvalue bound estimate without changing the rounding error analysis. For a stationary random field, σ is constant across the field. Then a scalar factor of σ^2 can be taken from $\mathbf{C}$ so:

$$\mathbf{C} = \sigma^2\mathbf{R} \tag{24}$$

where $\mathbf{R}$ is the correlation matrix with entries bounded between -1 and 1.

From Eq. (19), $\mathbf{C}\mathbf{Q} = \mathbf{Q}\mathbf{\Lambda} = \sigma^2\mathbf{R}\mathbf{Q}$ so:

$$\mathbf{R}\mathbf{Q} = \sigma^{-2}\mathbf{Q}\mathbf{\Lambda} \tag{25}$$

Then, with reference to Eq. (19), the eigenvalues of $\mathbf{R}$ are proportional to $\sigma^{-2}\mathbf{\Lambda}$. From the discussion in Section 3.2.2, taking the eigenvalue decomposition of $\mathbf{C}$ gives eigenvalues proportional to σ^2. Then the eigenvalues of $\mathbf{R}$ are proportional to unity. From this the largest eigenvalue, $\lambda_{\max}(\mathbf{C})$, for a stationary random field is:

$$\lambda_{\max}(\mathbf{C}) \lesssim \sigma^2 \tag{26}$$

3.2.2. Random field simulation by eigenvalue decomposition for positive definite covariance matrices

Although not used directly for the analysis in Section 4, it is instructive to examine the generation of random fields first by eigenvalue decomposition. This decomposition is one of several possible decompositions of the covariance matrix that can be used to generate random fields. First, the simpler case of a positive definite matrix is considered.

In infinite precision arithmetic, a positive definite covariance matrix may occur, for example, when the covariance function is monotonically decreasing. By Definition 6.1.9 in [24], a matrix is strictly diagonally dominant if the diagonal entries are strictly greater than all other entries in the matrix. By Theorem 6.1.10, Conditions a and b of [24], a strictly diagonally dominant matrix is non-singular and has positive real eigenvalues. If the covariance function is monotonically decreasing, as is the case in the analysis in Section 4, the diagonal entries in the covariance matrix are always greater than the diagonals as the largest correlation occurs between an element and itself.

Even in the case of a monotonically decreasing correlation function, finite precision arithmetic may result in the covariance matrix becoming diagonally dominant, rather than strictly diagonally dominant. Then the diagonal entries are greater than or equal to the rest of the entries in the matrix. Indeed, if care is not taken with algorithms, diagonal dominance can be lost completely. Numerical stability issues are addressed in Section 3.4.

Given an $n \times n$ positive definite covariance matrix decomposed into eigenvectors and eigenvalues as $\mathbf{C} = \mathbf{Q}\mathbf{\Lambda}$, a sample from Gaussian random field, $Z(x, y)$, can be generated:

$$Z(x, y) = \mathbf{Q}\mathbf{\Lambda}^{(1/2)}a + \mu \tag{27}$$

where a is a vector of size n whose entries are given by random samples of a standard normal distribution and μ is the mean of the random field [45,14].

Eq. (27) can be understood as generating a random field in three steps. First a set of n uncorrelated, unit length random degrees of freedom are scaled relative to each other by $b = \mathbf{\Lambda}a$. This can be thought of as generating a series of ellipses with principal axes aligned with the canonical basis vectors. Then each b represents a set of uncorrelated samples from Gaussian distributions such that b_i has standard deviation $\sqrt{\lambda_i}$. In the case that the matrix is positive definite, $\sqrt{\lambda_i}$ is always strictly greater than zero. The implication of this is that each random degree of freedom, in this representation, is linearly independent.

Multiplication by orthogonal matrices rotates a set of vectors while preserving the lengths and angles between the vectors [18]. The second step in generating a random field sample by this method is then multiplication of b by $\mathbf{Q}$ to rotate the scaled, uncorrelated vectors b to the correct correlation required for $Z(x, y)$. The rotation of the principal axes of the ellipses mentioned previously, relative to the canonical basis vectors, describes the correlation between the random variables of $Z(x, y)$. The shape of the ellipse also changes, becoming more eccentric as the rotation increases [30]. The third and final step is the addition of the scalar valued mean function, μ to each point within the random field.

3.2.3. Random field simulation by Cholesky decomposition for positive definite covariance matrices

The Cholesky decomposition can be computed more quickly than an eigenvalue decomposition and thus can be used to improve

the run time of a covariance matrix decomposition based random field generator. This is discussed in more detail in Section 3.3.

Given a symmetric, positive definite matrix **C**, the Cholesky decomposition algorithm can be used to decompose **C** into a lower triangular matrix **L** such that:

$$\mathbf{C} = \mathbf{L}\mathbf{L}^{\mathbf{T}} \tag{28}$$

where T denotes the matrix transpose. Various algorithms implementing the Cholesky decomposition can be found in [18].

A random field can be generated using **L**. After calculating **L** given Eq. (28), the random field $Z(x,y)$ can be obtained by:

$$Z(x,y) = \mathbf{L}a + \mu \tag{29}$$

where a is a vector of size n whose entries are given by random samples of a standard normal distribution. Eq. (29) gives a single value of a random field per finite element. To generate additional random field realisations for Monte Carlo Simulation it is necessary to retain **L** between simulations. For each realisation, a new vector of random samples a is generated and multiplied with **L** as per Eq. (29).

In a rough sense, the Cholesky decomposition takes the 'square root' of a matrix (although the square root of a matrix is not necessarily equal to **L** [18]). Recall from the previous section that the eigenvectors of **C** can be thought of as representing the principal axes, with magnitude σ, of a set of ellipses. In contrast, **L** describes the same ellipses in a different form. The column and row vectors of **L** are the direction of the linear regression lines of one column vector over all others [37,30,16]. Let $Z(i)$ denote the value of the random field associated with the element in the discretisation mesh with index i. Also, let L_i denote the i-th row vector of **L**. Then, more simply, each L_i describes the random variable associated with $Z(i)$. If the correlation between some $Z(i)$ and $Z(j)$ is ρ, then correlation between these degrees of freedom is equal to:

$$\rho_{x,y} = \cos\theta \tag{30}$$
$$\phi = \frac{\pi}{4} + \frac{\theta}{2}$$

where θ is the angle between the two possible regression lines describing the ellipses for $Z(i)$ and $Z(j)$ and ϕ is the angle between vectors L_i and L_j [8,16].

To see how a random field is constructed by Eq. (29), consider the following. **L** is a lower triangular matrix and so for a row j, all entries in columns greater than j are zero. Consider the result of $Z(x,y) = \mathbf{L}a$. The first two entries will be:

$$Z(x,y)_1 = \mathbf{L}_{1,1} \times a_1 + 0$$
$$Z(x,y)_2 = \mathbf{L}_{2,1} \times a_1 + \mathbf{L}_{2,2} \times a_2 + 0$$

As the ordering of elements in the random field is arbitrary, the row ordering of **C** should not impact on the final result. The first degree of freedom in the random field is taken up by a_1, the choice of which element is represented by a_1 is arbitrary. The second degree of freedom also represents an arbitrary element. Ignoring other elements in the random field, a_2 only needs to be correlated to itself and the first degree of freedom. Proceeding in this manner, the uncorrelated a values are assigned the correct correlation structure.

3.2.4. Random field simulation by Cholesky decomposition for positive semi-definite (singular) covariance matrices

The eigenvalues of the covariance matrix, **C** may become zero, or even negative, as a result of finite precision arithmetic and associated rounding errors. Additionally, even in theoretical infinite precision mathematics, if the covariance function is constant then linear dependencies between the columns of **C** may occur and **C** will be positive semi-definite. As a result, the covariance matrix may become singular, or will be in the case of linear dependence. In this section a method to generate random fields in the event that the covariance matrix is singular is presented. An analysis of the errors of this method is presented in Section 3.4.

Methods exist to ensure that the covariance matrix is positive semi-definite. Naive modifications to the Cholesky decomposition matrix can remove negative eigenvalues by adding a small error term to the main diagonal. This ensures diagonal dominance. More sophisticated variations on such a technique and the associated error bounds are detailed in [11,5].

With negative eigenvalues removed, the $n \times n$ covariance matrix, **C**, may be positive semi-definite and therefore singular. A method for resolving this problem is given in [2], which is discussed here. A modification of the results in [2] to allow generating random field samples when the covariance matrix is singular is presented. First, recall that by Eq. (23), the number of linearly independent columns of **C** is equal to $n-k$ where k is the multiplicity of zero eigenvalues, as in Eq. (20). To find a useful decomposition of **C**, it is possible to split the singular and non-singular parts of **C**. The following procedure is from [2]. First reorder the columns of **C** such that the first $p = n - k$ columns are linearly independent. Then it is possible to write:

$$\mathbf{C} = [\mathbf{C}_I \quad \mathbf{C}_D]$$

where $\mathbf{C}_I$ is an $n \times p$ matrix and $\mathbf{C}_D$ is $n \times (n-p) = n \times k$ so:

$$\mathbf{C}_D = \mathbf{C}_I\mathbf{B}$$

where **B** is size $p \times k$. Also, $\mathbf{C}_I$ can be split into an upper $p \times p$ part, $\mathbf{C}_{IU}$, and a lower $k \times p$ part, $\mathbf{C}_{IL}$. Then:

$$\mathbf{C} = \begin{bmatrix} \mathbf{C}_{IU} & \mathbf{C}_{IU}\mathbf{B} \\ \mathbf{C}_{IL} & \mathbf{C}_{IL}\mathbf{B} \end{bmatrix}$$

Then, as **C** is symmetric, $\mathbf{C}_{IL}^T = \mathbf{C}_{IU}\mathbf{B}$ and then finally:

$$\mathbf{C} = \begin{bmatrix} \mathbf{C}_{IU} & \mathbf{C}_{IU}\mathbf{B} \\ \mathbf{B}^T\mathbf{C}_{IU}^T & \mathbf{B}^T\mathbf{C}_{IU}^T\mathbf{B} \end{bmatrix} \tag{31}$$

In this form, **C** can be made from just two parts. $\mathbf{C}_{IU}$ is a non-singular $p \times p$ matrix and **B** contains the coefficients describing the linear dependencies between the columns of $\mathbf{C}_{IU}$. A numerical example is given in [2]. To find $\mathbf{C}_{IU}$ and **B**, the first step is to find the linearly dependent columns of **C**. From Lemma 12.2 of [19], two column vectors, x and y are linearly dependent if:

$$\begin{vmatrix} x \cdot x & x \cdot y \\ y \cdot x & y \cdot y \end{vmatrix} = 0 \tag{32}$$

where $|\mathbf{A}|$ is the determinant of **A** and $x \cdot y$ is the scalar product of x and y.

The linear dependencies in **C** can be found by comparing columns from left to right. Let the column vectors of **C** be $C_1, \ldots C_n$. Start by comparing C_1 with all columns C_i for $1 < i \leqslant n$. Then compare C_2 with all C_i for $2 < i \leqslant n$. Once a C_i has been found to be linearly dependent, it can be excluded from subsequent checks. Continuing in this fashion, the linear dependence of all columns can be checked. If two columns, say C_j and C_k with $j < k$ are found to be dependent, a new row is made in **B** to represent column C_j and a new column to represent C_k. The corresponding entry into **B** is the factor ω_{jk}, from:

$$C_k = \omega_{jk}C_j \tag{33}$$

After the entries of **B** are filled in, $\mathbf{C}_{IU}$ is formed by deleting k dependent rows and columns from **C**. Specifically, for each column C_k that is linearly dependent on a C_j with $j < k$, delete both row and column k from **C**.

A random field sample can now be generated using $\mathbf{C}_{IU}$ and $\mathbf{B}$. For the non-singular part $\mathbf{C}_{IU}$, the procedure in Section 3.2.3 can be applied. Let $\mathbf{L}_{IU}$ be the lower triangular matrix produced by applying the Cholesky decomposition to $\mathbf{C}_{IU}$. Then, as in Eq. (29), $Z(x,y) = \mathbf{L}_{IU}a_I + \mu$ where a_I is of size $p = n - k$. This gives part of the random field sample.

To complete the sample, the linear dependencies described by $\mathbf{B}$ must be included. From the discussion in Section 3.2.3, the degree of correlation between two random degrees of freedom is represented in the covariance matrix by the angle between the two representative basis vectors. When the basis vectors are linearly dependent they are, by definition, collinear. Then linear dependence between basis vectors also indicates perfect correlation between these degrees of freedom. As in Eq. (33), let each C_k be linearly dependent on some C_j. Then $\mathbf{B}^T\mathbf{L}_{IU}a_I + \mu$ gives the value of the random field for each of the k linearly dependant elements.

Let $Z(i)$ be the value of the random field over the discrete element with index i. Then a random field can be generated from a singular covariance matrix by a modified Cholesky decomposition by:

$$Z(i) = \mathbf{L}_{IU}a_I + \mu \tag{34}$$

$$Z(k) = \mathbf{B}^T\mathbf{L}_{IU}a_I + \mu \tag{35}$$

where the $Z(i)$ entries come from the non-singular degrees of freedom contained in $\mathbf{C}_{IU}$ and the $Z(k)$ are linearly dependant on the $Z(i)$ parts of the random field sample.

In practice, it is preferable to first run a rank-revealing Cholesky decomposition as in [18,23]. Such a decomposition fills in the entries of $\mathbf{L}_{IU}$, reordering the columns $\mathbf{C}$ as necessary, until the diagonals of $\mathbf{L}_{IU}$ become sufficiently small. Once this cut off, ϵ, is reached after $\text{rank}(\mathbf{L}_{IU}) \approx p$, the remaining k columns can be scanned for linear dependencies to fill in the entries of the $\mathbf{B}$ matrix. If $\mathbf{B}$ is filled in first, then there may be no linear dependencies and therefore computer time is wasted for no gain. By computing a rank-revealing Cholesky decomposition first, if $\mathbf{C}$ is non-singular so $\text{rank}(\mathbf{L}_{IU}) = n$, then there is no need to expend computation effort searching for linear dependencies.

3.3. Computational complexity of RFEM combined with covariance matrix decomposition

RFEM relies on the generation of both a very large number of both random field samples and the solution of finite element problems. Assessing the computational requirements is a useful tool to check that a procedure is feasible.

Before discussing this, the following brief note on some required notation is necessary. To estimate the computational complexity of algorithms, it is useful to adopt big-O notation as in [9]. To count the time to complete an algorithm, each floating point operation (flop) is summed. An algorithm may take, for example, $\mathcal{O}(n^5) \approx 7n^5 + 6n^2$ flops to complete where n is the number of inputs. In big-O notation, coefficients are dropped and only the dominating terms as n approaches infinity are retained.

3.3.1. Computational complexity of covariance matrix decomposition

For the analysis in Section 4, a Cholesky decomposition was preferred over an eigenvalue decomposition. Both the Cholesky and eigenvalue decompositions take roughly $\mathcal{O}(n^3)$ flops [18]. However, Cholesky decomposition can be completed in approximately $n^3/3$ flops versus $4n^3/3$ for a typical tridiagonal QR based eigenvalue decomposition [18]. While asymptotically the runtime of the two algorithms is the same, the speed of the Cholesky decomposition is beneficial.

To generate a set of random fields for RFEM analysis using covariance matrix decomposition, the decomposition need only be completed once. After the initial $\mathcal{O}(n^3)$ decomposition, a random field sample can be generated rapidly. For example, with Cholesky decomposition, as in Eq. (29), the vector a and multiplication with the lower triangular matrix $\mathbf{L}$ is required. a can be generated in $\mathcal{O}(n)$ flops. Multiplication of a vector with a lower triangular matrix is also fast, taking just $\mathcal{O}(n^2)$ flops [18].

If the covariance matrix is singular, then the procedure in Section 3.2.4 can be applied to find and delete linear dependencies. Calculating a scalar product of two vectors takes $\mathcal{O}(n)$ flops [18]. Then computing Eq. (32) takes $4\mathcal{O}(n) + 5 \approx \mathcal{O}(n)$ flops. To find all linear dependencies, each column must be iterated over from left to right, taking $\mathcal{O}(n)$ work. Then from column C_i, columns C_j for $i < j \leqslant n$ must be iterated over, also taking $\mathcal{O}(n)$. Then the total complexity of the column elimination algorithm is $\mathcal{O}(n^3)$ and is therefore not asymptotically any worse than the decomposition itself. If a parallel and block matrix approach was taken for very large n, then care would need to be taken to minimise the overhead associated with moving data, such as reordering columns.

The total computational complexity of random field generation by covariance matrix decomposition is then:

$$\mathcal{O}(n^3) + m \cdot \mathcal{O}(\text{FEM}) \cdot \mathcal{O}(n^2) \tag{36}$$

where m is the number of MCS iterations used for RFEM and $\mathcal{O}(\text{FEM})$ is the complexity of each finite element analysis. These components are discussed in the following sections.

3.3.2. Computational complexity of finite element analysis

The computational complexity of finite element analysis is discussed in [39] and summarised in [12]. Linear elastic FEM takes approximately $\mathcal{O}(nw^2)$ where n is the number of input elements and w is the stiffness matrix bandwidth. The bandwidth term reflects the fact that stiffness matrices are often sparse, that is, mostly filled with zeroes. If plastic, non-linear FEM is used, then a number of load steps, l must be carried out. Then:

$$\mathcal{O}(\text{FEM}) = \mathcal{O}(nw^2l) \tag{37}$$

where l is low for a convergent problem and higher for an unstable problem.

3.3.3. Computational complexity of RFEM

Combining Eqs. (36) and (37), the following total complexity of RFEM is obtained:

$$\mathcal{O}(\text{RFEM}) = \mathcal{O}(n^3) + m \cdot \mathcal{O}(nw^2l) \cdot \mathcal{O}(n^2)$$

This can be simplified to:

$$\mathcal{O}(\text{RFEM}) = \mathcal{O}(mn^3w^2l) \tag{38}$$

Then the following point can be made, the computational complexity of RFEM by covariance matrix decomposition is not limited by the decomposition itself. It is the MCS finite element iterations which are the bottle neck. Consider, for example an FFT based random field generator. In two dimensions, this takes $\mathcal{O}(n^2 \log n)$ work [14,9]. This work must be carried out for each of the k MCS iterations. In this case, $\mathcal{O}(\text{RFEM}) = k \cdot \mathcal{O}(n^3w^2l \log n)$. LAS has a similar run time complexity to FFT, taking 1.5 to 2 times longer per realisation in two dimensions [15]. Thus LAS has a similar asymptotic run time to FFT. As such, the choice of random field generator is not the computationally limiting factor for RFEM. Rather, the Monte Carlo FEM iterations are the most significant computational cost, especially for large m.

3.4. Precision of RFEM with covariance matrix decomposition

3.4.1. Preliminaries

Finite precision arithmetic carries round off errors. The numerical precision of covariance matrix decomposition random field

sampling for use with RFEM is addressed. Specifically, an estimate of the roundoff errors associated with the generation of stationary random fields by Cholesky decomposition for RFEM is given.

The error analysis presented requires the concept of backward and forward errors. First, consider a simple calculation $y = f(x)$. Let $\hat{y}$ denote the finite precision approximation to y. Then $\hat{y} = f(x + \Delta x)$ and Δx is termed the backward error. Let $x + \epsilon$ be some measured quantity, where ϵ is the error in x. If $\Delta x \ll \epsilon$ then it is difficult to reject the computed $\hat{y}$ on the basis of finite precision rounding errors. Similarly, the forward error is given by $y - \hat{y} = \Delta y$.

Modern computers use the IEEE standard 754 for binary floating point arithmetic. The 64 bit double precision type is used for this paper. From [23], the unit roundoff, u, for a double is defined to be:

$$u = 2^{-53} \approx 1.11 \times 10^{-16} \tag{39}$$

The vector two norm and the matrix two and Frobenius norms are required. From [18], the vector two norm is defined, for some vector x of length n, as:

$$\|x\|_2 = \left(\sum_{i=1}^{n} |x_i|^2 \right)^{(1/2)} \tag{40}$$

Also from [18], the matrix two and Frobenius norms are, for some $n \times n$ matrix $\mathbf{A}$, defined as:

$$\|\mathbf{A}\|_2 = \lambda_{\max}(\mathbf{A}) \tag{41}$$

$$\|\mathbf{A}\|_F = \left(\sum_{i=1}^{n} \sum_{j=1}^{n} |A_{i,j}|^2 \right)^{(1/2)} \tag{42}$$

The following inequalities from [23] are also useful:

$$\|\mathbf{A}\|_F \leqslant \sqrt{\operatorname{rank}(\mathbf{A})} \|\mathbf{A}\|_2 \tag{43}$$

$$\|\mathbf{A}\|_2 \leqslant \|\mathbf{A}\|_F \tag{44}$$

To generate a random field as in Eq. (29), a Cholesky decomposition followed by a matrix–vector multiplication is required. Let $\hat{Z} = \hat{\mathbf{L}}a + \mu$ be the computed random field sample in finite precision arithmetic. The roundoff error for the addition of μ is of size u and negligible and will be ignored for the remainder of the error analysis.

3.4.2. Random field sample error bounds covariance matrix decomposition

The error associated with the Cholesky decomposition is considered. First, the case of a positive definite $\mathbf{C}$ is analysed. The backward error is given by $\Delta\mathbf{C}$ where:

$$\hat{\mathbf{L}}\hat{\mathbf{L}}^T = \mathbf{C} + \Delta\mathbf{C}$$

From Section 10.1.1 of [23]:

$$\|\Delta\mathbf{C}\|_2 \leqslant \mathcal{O}(n^2 u) \|\mathbf{C}\|_2 + \mathcal{O}(u^2) \tag{45}$$

By Eq. (26), an estimate for $\|\mathbf{C}\|_2$ is:

$$\|\mathbf{C}\|_2 \lesssim \sigma^2$$

For a stationary random field, $\sigma^2\mathbf{R} = \mathbf{C}$. The Cholesky decomposition can be calculated for $\mathbf{R}$ and then each of the independent degrees of freedom scaled by σ. By ordering the calculations this way, the forward error estimates can be reduced. To demonstrate this, calculations of bounds for both $\mathbf{R}$ and $\mathbf{C}$ are included. An estimate for $\|\mathbf{R}\|_2$ is:

$$\|\mathbf{R}\|_2 \lesssim 1$$

From Section 4.2.6 of [18], $\|\mathbf{L}\|_2^2 = \|\mathbf{C}\|_2$ so:

$$\|\mathbf{L}\|_2 \lesssim \sigma \tag{46}$$

For a stationary random field, if the decomposition is done using $\mathbf{R} = \mathbf{L}_\mathbf{R}\mathbf{L}_\mathbf{R}^T$, then:

$$\|\mathbf{L}_\mathbf{R}\|_2 \lesssim 1 \tag{47}$$

The backward error in $\mathbf{C}$ can be estimated from the above equations. Additionally, the result below holds for all (not just positive definite) $\mathbf{C}$ if the algorithms in [11] are adopted. The backward error in $\mathbf{C}$ and $\mathbf{R}$ is then:

$$\|\Delta\mathbf{C}\|_2 \lesssim \mathcal{O}(n^2 u)\sigma^2 \tag{48}$$

$$\|\Delta\mathbf{R}\|_2 \lesssim \mathcal{O}(n^2 u) \tag{49}$$

Combining Eqs. (43), (48) and (49):

$$\|\Delta\mathbf{C}\|_F \lesssim \mathcal{O}(n^{(3/2)})u\sigma^2$$

$$\|\Delta\mathbf{R}\|_F \lesssim \mathcal{O}(n^{(3/2)})u$$

This gives the following useful result:

$$\frac{\|\Delta\mathbf{C}\|_F}{\|\mathbf{C}\|_2} \lesssim \mathcal{O}(n^{(3/2)})u \tag{50}$$

The forward error of the Cholesky decomposition is given by $\Delta\mathbf{L} = \mathbf{L} - \hat{\mathbf{L}}$. From Theorem 10.8 of [23,4]:

$$\frac{\|\Delta\mathbf{L}\|_F}{\|\mathbf{L}\|_2} \leqslant \mathcal{O}(\kappa_2(\mathbf{C})) \frac{\|\Delta\mathbf{C}\|_F}{\|\mathbf{C}\|_2} \tag{51}$$

where $\kappa_2(\mathbf{C})$ is the condition number of $\mathbf{C}$. A large condition number represents an ill-conditioned system. Let $\lambda_{\max}(\mathbf{C})$ and $\lambda_{\min}(\mathbf{C})$ be the maximum and minimum eigenvalues of $\mathbf{C}$ respectively.

From Section 4.2.6 of [18], as $\mathbf{C}$ is symmetric positive definite:

$$\kappa_2(\mathbf{C}) = \frac{\lambda_{\max}(\mathbf{C})}{\lambda_{\min}(\mathbf{C})} \tag{53}$$

Bounds for $\kappa_2(\mathbf{C})$ can be derived if a rank-revealing decomposition, as discussed in Section 3.2.4, is used. Then, from Section 10.1.1 of [23], the decomposition will succeed if $20n^{(3/2)}\kappa_2(\mathbf{C})u \leqslant 1$. Then, for the linearly independent part $\mathbf{C}_{IU}$:

$$\kappa_2(\mathbf{C}_{IU}) \leqslant \frac{1}{20n^{(3/2)}u} \tag{54}$$

This gives a lower bound estimate for $\lambda_{\min}(\mathbf{C}_{IU})$:

$$\lambda_{\min}(\mathbf{C}_{IU}) \gtrsim \mathcal{O}(n^{(3/2)}u)\sigma^2 \tag{55}$$

or for a stationary random field:

$$\lambda_{\min}(\mathbf{R}_{IU}) \gtrsim \mathcal{O}(n^{(3/2)}u) \tag{56}$$

The error bound in Eq. (51) is affected by the size of $\kappa_2(\mathbf{C})$ and may be as bad as $\mathcal{O}(\kappa_2(\mathbf{C})u)$ for a general symmetric positive definite matrix [23].

An improved error bound estimate can be made investigating the structure of covariance matrices. From Eq. (30), the correlation between two random degrees of freedom, represented by vectors x and y, in a random field is given by the relative angle between them. The angle between two independent degrees of freedom is at most $\pi/2 \approx \mathcal{O}(1)$. As the x and y become collinear, the angle between them approaches zero. Additionally, as x and y become collinear $\mathbf{C}$ approaches singularity and one of the eigenvalues of the system approaches 0.

From [30], the equation of the ellipse described by two column vectors L_i and L_j of $\mathbf{L}_{\mathbf{R}IU}$, with correlation $\rho = \cos\theta$ as in Eq. (30) is:

$$x_1^2 - 2\rho x_1 x_2 + x_2^2 = (1 - \rho^2)$$

$$x_1^2 - 2\cos\theta x_1 x_2 + x_2^2 = \sin^2\theta \tag{57}$$

where x_1 and x_2 are canonical basis vectors. Let A be the area of the ellipse given by Eq. (57). For the implicit equation of an ellipse in the form $a_1 x_1^2 + a_2 x_1 x_2 + a_3 x_2^2 = 1$, the area of the ellipse is:

$$A = \frac{2\pi}{\sqrt{4a_1a_3 - a_2^2}}$$
$$A = \frac{2\pi}{\sqrt{4\left(\frac{1}{\sin^2\theta}\right)^2 - \left(\frac{-2\cos\theta}{\sin^2\theta}\right)^2}}$$
$$A = \frac{2\pi}{\sqrt{\left(\frac{4}{\sin^4\theta}\right)(1-\cos^2\theta)}}$$
$$A = \frac{2\pi}{\sqrt{\frac{4}{\sin^2\theta}}}$$
$$A = \pi\sin\theta \tag{58}$$

The area of an ellipse is also, however, given by $A = \pi a * b$ where a and b are the lengths of the semi-major axes of the ellipse. From [16] and the discussion in Section 3.2.2, for $\mathbf{R}_{IU}$, the length of semi-major axes of the ellipse are equal to $\sqrt{\lambda_1}$ and $\sqrt{\lambda_2}$ where λ_1 and λ_2 are the eigenvalues corresponding to the random degrees of freedom that represent elements i and j. Then:

$$\sin\theta = \sqrt{\lambda_1\lambda_2} \tag{59}$$

The eccentricity of an ellipse with semi-major axis lengths a and b with $b \leqslant a$ is defined as $e = \sqrt{1 - b^2/a^2}$. By definition, $e = 0$ for a circle and $e < 1$ for an ellipse. So when $\lambda_1 = \lambda_2$, $\sin\theta = 0$. Then as θ increases, $\sqrt{\lambda_1\lambda_2}$ must also increase. As θ approaches the maximum of $\pi/2$, $\sin\theta$ approaches 1. Then increasing λ_1 must decrease λ_2 and vice versa. From Eqs. (24)–(26), $\lambda_{\max}(\mathbf{R}_{IU})$ and $\lambda_{\min}(\mathbf{R}_{IU})$ are bounded between $\lambda_{\min}(\mathbf{R}_{IU})$ and 1. Fixing $\lambda_1 = \lambda_{\max}(\mathbf{R}_{IU})$:

$$\theta \to \frac{\pi}{2}, \quad \lambda_2 \to \lambda_{\min}(\mathbf{R}_{IU}) \tag{60}$$

Let $\psi_{\min}$ be the minimum angle, as in Eq. (30), between two correlated degrees of freedom represented by vectors x and y. Then the maximum error, δ, in the distance of y from x is:

$$\delta \approx \alpha\sin\psi_{\min}$$
$$\delta \approx \alpha\mathcal{O}(\psi_{\min}) \tag{61}$$

where α is the distance moved along y. So:

$$\sin\psi_{\min} \approx \sqrt{\lambda_{\max}(\mathbf{R}_{IU})\lambda_{\min}(\mathbf{R}_{IU})} \tag{62}$$

In standard IEEE 754 floating point arithmetic, there is no loss of precision for the square root operation [26]. Then, if the lower bound in Eq. (56) is satisfied, the precision of $\sqrt{\lambda_{\min}}$ is roughly the same as that of $\lambda_{\min}$:

$$\sqrt{\lambda_{\min}} \approx \mathcal{O}(n^{(3/2)}u) \tag{63}$$

Combining Eqs. (62) and (63):

$$\mathcal{O}(\psi_{\min}) \approx \alpha\mathcal{O}(n^{(3/2)}u) \tag{64}$$

From Eq. (34), random field is generated by multiplying $\mathbf{L}_{\mathbf{R}IU}$ by a vector, a, of n samples from a standard normal distribution. Each value in the final random field is then generated by moving a distance a_i along at most n of the random degrees of freedom described by the row vectors of $\mathbf{L}_{\mathbf{R}IU}$. From Eq. (64), the error in each of these n multiplications is:

$$a_i\mathcal{O}(n^{(3/2)}u) \tag{65}$$

To make use of Eq. (65), an estimate for the magnitude of each a_i is needed. Technically each a_i is unbounded as it is a sample from a standard normal distribution, and therefore the theoretical upper bound of $|a_i|$ is infinite. However, it would be exceedingly unlikely for each of the n entries in a to be much more than ± 3 and certainly less than say ± 100. Then, a practical estimate for $|a_i|$ is:

$$|a_i| \lesssim \mathcal{O}(10) \tag{66}$$

Note that the result of the multiplication $\mathbf{L}_{\mathbf{R}}a$ must be increased by a factor of σ to scale the random field to the correct standard deviation. By Section 2.7.8 of [18], the error associated with scalar multiplication is approximately $\mathcal{O}(u\sigma\|\mathbf{L}_{\mathbf{R}}\|) \approx \mathcal{O}(u\sigma)$. Then, for a stationary random field, decomposing $\mathbf{R}$ and multiplying $\mathbf{L}_{\mathbf{R}IU}a$ by σ only scales up the error in $\mathbf{L}_{\mathbf{R}IU}a$ by approximately σ. Then the roundoff error, $\Delta Z = Z - \hat{Z}$, for entry, $Z(i)$, in the random field sample is approximately:

$$\Delta\hat{Z}(i) \lesssim 10\sigma n\mathcal{O}(n^{(3/2)}u)$$
$$\Delta\hat{Z}(i) \lesssim \sigma\mathcal{O}(10n^{(5/2)}u) \tag{67}$$

For a singular correlation matrix, if the procedure in Section 3.2.4 is adopted, all random degrees of freedom separated by less than $\psi_{\min}$ are considered collinear. Then, by a similar argument above, the maximum angular error between two degrees of freedom, r and s, is $\psi_{\min}$. If the angular error were more than this, then the λ_2 for the ellipse representing r and s would be larger than $\lambda_{\min}\mathbf{L}_{\mathbf{R}IU}$ and r and s would not be numerically collinear. Then if the angular error for assumed collinear degrees of freedom is at most $\psi_{\min}$, then the same error given by Eq. (67) holds.

Finally, the magnitude of the variance reduction γ needs to be considered. The actual magnitude of the minimum eigenvalue of $\mathbf{R}$ is:

$$\lambda_{\min}(\mathbf{R}_{IU}) \approx \frac{\mathcal{O}(n^{(3/2)u})}{\gamma_{\min}} \tag{68}$$

If the magnitude of $\gamma_{\min}$ is greater than approximately 0.5, the magnitude of the error in $\lambda_{\min}(\mathbf{R}_{IU})$ is unchanged. So then to maintain the precision estimates given in this section, the following bound on the minimum variance reduction should be adopted as:

$$\gamma_{\min} \geqslant 0.5 \tag{69}$$

From Eq. (67) and u as in Eq. (39), the rounding error can be estimated for different n:

$$\text{For } n \approx 10^3, \quad |\Delta\hat{Z}| \lesssim 10^{-8}\sigma$$
$$\text{For } n \approx 10^4, \quad |\Delta\hat{Z}| \lesssim 10^{-5}\sigma$$
$$\text{For } n \approx 10^5, \quad |\Delta\hat{Z}| \lesssim 10^{-3}\sigma$$

Note that these error estimates are very rough and represent a worst case scenario without any attempt to alleviate rounding errors by, say, iterative refinement as in [23,18].

3.4.3. Rounding errors in FEM

To complete the error analysis of the covariance matrix decomposition random field generator, the rounding errors of FEM are discussed. Aside from measurement errors in the inputs, there are several sources of error in FEM. These sources of error include the fineness of the mesh (h-refinement), degree of the approximating polynomials (p-refinement) and the machine precision unit round off u.

Error estimates for the maximum theoretical precision of FEM, sufficient for the approximate bounds in this paper, are given in Section 6.8.3 of [42]. Although increasing h improves the accuracy of the computed FEM solution as $\mathcal{O}(h^{-2})$, eventually rounding errors prevent finer mesh elements from improving accuracy. Let q be the order of the finite element approximating polynomial. Then the maximum theoretical precision of FEM, δ is approximately:

$$\delta \approx \mathcal{O}(u^{(q+1)/(q+3)}) \tag{70}$$

Then, from [42], the estimates for the best case precision for FEM are:

For $q = 1$, $\delta \approx 10^{-8}$

For $q = 2$, $\delta \approx 10^{-10}$

For $q = 3$, $\delta \approx 10^{-11}$

Further, for implicit plastic finite element analysis, some form of residual convergence tolerance must be specified. The rounding errors in plastic FEM are at least as large as the specified tolerance [3].

3.5. Discussion and conclusions

The error and computational complexity characteristics of RFEM using covariance matrix decomposition as a random field generator were discussed. The computational complexity of the repeated FEM iterations were found to be the computationally limiting factor for RFEM, not the random field generator. Also, bounds on the rounding errors for FEM and Cholesky decomposition were discussed. The rounding errors for Cholesky decomposition, without error reducing techniques, may become problematic for 10^4 or 10^5 elements. However, for this many elements, an RFEM analysis, particularly for a high probability of failure, will be very time consuming. For a specific problem, the bounds presented in this paper may help to estimate the approximate size of a feasible solution compared to the rounding errors. It is also worth noting that the measurement accuracy for a geotechnical problem is likely to be worse than any rounding errors for a reasonable problem. Additionally, improving the p order of the finite element approximation allows for the number of elements to be reduced, which would lessen errors in the random field sample.

Without significant modifications, the methods presented are limited to Gaussian random fields and those derived from simple transformations of Gaussian random fields, for example, log-normal random fields. The same is true of most random field simulation techniques [38] and the simulation of non-Gaussian random fields remains an active area of research. As such, this limitation of matrix decomposition is not considered to be major.

Covariance matrix decomposition could also be used to generate random field samples for meshes of mixed elements. Rectangular local average and variance reduction formulas are known [14] and triangular formulas are provided in this paper. It would be a simple task, given the results of this paper to generate a mixed mesh quadrature approximation for local averaging variance reduction.

4. Analysis of a drained slope

4.1. Introduction

The validity of the methodology presented for random field simulation and discretisation for meshes of arbitrary triangular finite elements was implemented by the authors in the computer program NIRFS. The validity of the program was tested by comparing the results of a reliability assessment computed by NIRFS to published results. Ji et al. [27] present the results of a reliability assessment of a soil slope whereby failure is detected by means of a limit equilibrium analysis based on the probabilistic critical slip surface. Ji et al. [27] adopt two techniques for random field simulation; the method of autocorrelated slices and the method of interpolated autocorrelations. Both of these methods make use of a Mohr–Coulomb failure criteria, in which the shear strength, s of a soil is given by two parameters, c (the soil cohesion, a stress) and ϕ (the angle of internal friction). The soil yields at the point when the shear stress at a point exceeds $s = c + \sigma \tan \phi$, where σ is the normal stress to the plane of shear.

In both methods presented by Ji et al. [27], random field techniques are used to model the parameters c and ϕ along the base of each slice of the slip surface considered. In order to compare the reliability computed by NIRFS (a finite element based method) to the results published by Ji et al. [27] (limit equilibrium), the finite element mesh was first refined using the shear strength reduction (SSR) technique in order to find the strength reduction factor (SRF) that most closely matched the factor of safety as computed by limit equilibrium techniques. By adjusting the finite element mesh used by NIRFS so that the deterministic SRF matched the deterministic factor of safety presented by Ji et al. [27], the methods could be compared. This is discussed in more detail in this section. It is also noted that to carry out Monte Carlo Simulations as per RFEM, NIRFS was coupled with a two-dimensional finite element program, Phase2 by Rocscience, for the deterministic solution of each discrete Monte Carlo Simulation problem.

4.2. Problem geometry and material property parameters

The geometry of the slope analysed in [27] is shown in Fig. 3. The material property parameters and their statistical properties are presented in Table 1. The autocorrelation properties are discussed later in Section 4.6. These are roughly the default variations adopted for most limit equilibrium analyses [25].

The following exponentially decaying autocorrelation function, as per [27], is adopted for all analyses:

$$\rho(x_1, y_1, x_2, y_2) = \exp\left(-\frac{|x_1 - x_2|}{\theta_x} - \frac{|y_1 - y_2|}{\theta_y}\right) = \exp\left(-\frac{\tau_x}{\theta_x} - \frac{\tau_y}{\theta_y}\right)$$

To match the parameters used in [27], a cross-correlation factor between c and ϕ of -0.5 was adopted for all analyses. Cross-correlation was simulated by the same method presented in [27]. As per [27], four sets of correlation lengths were tested and are presented in Table 2.

4.3. Deterministic analysis by limit equilibrium

Using Slide by Rocscience, the deterministic factor of safety was determined by Spencers Method to be 1.214. [27] found the deterministic factor of safety to be 1.226. While the source of the difference is unclear, the two values were considered to be similar enough to proceed.

The limit equilibrium analysis demonstrates the location of the deterministic critical slip surface (Fig. 4).

4.4. Mesh refinement using Shear Strength Reduction

To compare the results of NIRFS to the results presented by [27], the finite element mesh was refined until both the finite element solution and the limit equilibrium approaches were as equivalent as possible. Without this refinement, the differences in probability of failure as computed by NIRFS compared to the results published by [27] would be obfuscated by severe model differences. The aim of the work presented in this section was to refine the finite element mesh so as to minimise these model differences.

The comparison between the finite element model and the limit equilibrium model was made by determining the critical SRF via the SSR method for varying levels of mesh refinement and different numbers of convergence iterations of the Newton–Raphson finite element solution. The results of these analyses were used to determine the finite element mesh to be used when computing the probability of failure of the slope using NIRFS.

Deterministic finite element analysis, using the mean parameters as presented in Table 1, was used to compute the SRF for each mesh. The SRF was computed using Phase2 by Rocscience. For each

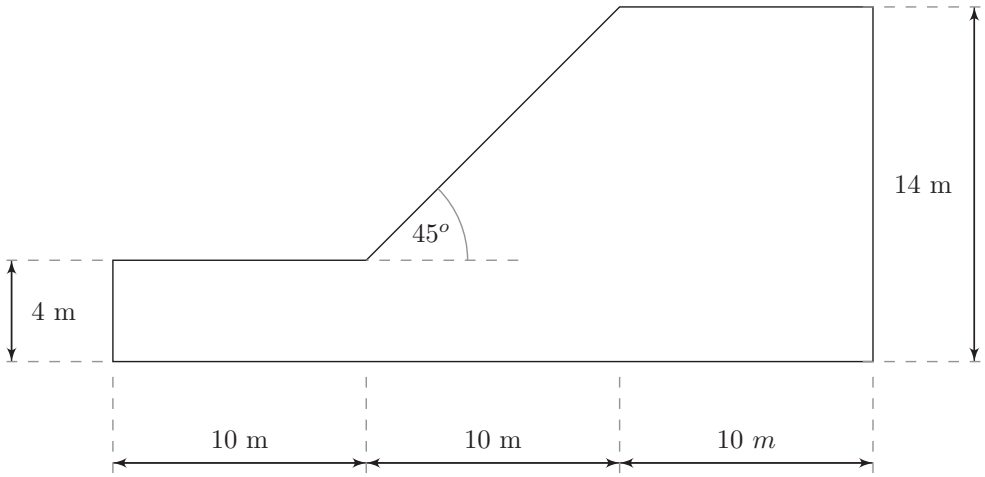

Fig. 3. Problem geometry: a homogeneous c–ϕ slope (from [27]).

Table 1
Statistical properties of soil parameters.

Parameter	Distribution	Mean	Standard deviation
Cohesion, c	Gaussian	15 kPa	4.5 kPa
Friction angle, ϕ	Gaussian	23°	2.3°
Unit weight, γ	Constant	19 kN/m^3	N/A

Table 2
Results of drained slope stability reliability analysis by NIRFS and [27]. Correlation lengths taken from [27].

Correlation length (m)		Probability of failure (%)		
θ_x	θ_y	Auto-correlated slices from [27]	Interpolated auto-correlations from [27]	NIRFS (20×10^3 simulations)
30	3	1.24	1.28	2.91
1000	3	1.54	1.71	3.67
30	1000	6.26	6.35	7.50
1000	1000	17.58	7.26	7.92

mesh refinement level considered, a study of the number of iterations to be used for the finite element solution was undertaken.

For this type of finite element problem, the SRF is equivalent to the factor of safety computed by limit equilibrium methods but is subject to fewer assumptions (e.g. interslice force issues) than limit equilibrium and is considered by practitioners to be the "best" estimate of factor of safety. The SSR method proceeds by iteratively altering the shear strength, $s = c + \sigma \tan \phi$ as:

$$s_r = \frac{s}{SRF}$$

The critical SRF value, SRF_c, is defined as the value at which the factor of safety of the slope is equal to one, that is, that the resisting and driving forces within the slope are in balance. To find SRF_c, trial values of SRF are used to calculate s_r. The slope is analysed for stability with the new value of s_r. If the slope fails, then SRF is too large. If the slope does not fail, SRF is too small. SRF_c can then be bounded to a value within some desired tolerance by repeated bifurcations of the current and previous values of SRF. For a more details see [22].

Five levels of mesh refinement were considered. The finite element meshes described above were analysed to determine the effect of the number of iterations undertaken by the finite element plastic solver on the critical SRF. Fig. 5 presents the results of these analyses.

The results in Fig. 5 indicate that the finite element mesh with 7112 elements, shown in Fig. 6, with a maximum of 5000 Newton–Raphson iterations would be the most appropriate for use with the NIRFS analysis. The SRF calculated (1.22) most closely matches the factor of safety computed by the limit equilibrium approach (1.21). Fig. 7 shows the contours of maximum shear strain at the critical SRF for the finite element mesh in Fig. 6 with 5000 iterations.

Fig. 5 also indicates that the computed SRF changes with both the level of mesh refinement as well as number of iterations (this effect was also observed in [41]). The figure indicates that for the mesh shown in Fig. 6, there is no benefit in increasing the number of iterations past 5000. The intent of this analysis was to determine the finite element mesh that gives the minimum difference between the limit equilibrium factor of safety and the SRF so as to enable a comparison between the probabilities of failure computed by NIRFS and the probabilities of failure found by [27]. By refining the finite element model, differences between the NIRFS and the approaches in [27] should be independent of the finite element mesh and convergence criteria. The tolerance of the similarity between the NIRFS model and the limit equilibrium models was found to within two decimal places. From the discussion in Section 3.4, any numerical precision errors in either FEM of the Cholesky decomposition will be much smaller than this error. As such, rounding errors are not sufficient to invalidate the analysis. The probability of failure, however, will only be precise to at most three significant figures.

4.5. Finite element variance reduction

Using the finite element mesh in Fig. 6, the variance reduction for each finite element can be computed using Eq. (11). This was carried out to determine if the variance reduction could be expected to have a large effect on the computed probabilities of failure for each set of correlation lengths given in Table 2. The intent was to reduce the variance reduction to minimise precision errors in the generated random fields, as discussed in Section 3.4.2 to allow comparison with the results by [27]. The effect of error due to excessive variance reduction was determined to be negligible for this particular mesh.

A twelve point Gaussian quadrature, using the weights given in [10] was adopted for each element. The variance reduction for each element in the finite element mesh in Fig. 6 for each correlation length set in Table 2 is presented in Fig. 8.

Fig. 8 indicates that as element area increases, the variance reduction increases over this area. Fig. 8 also indicates that as correlation length increases, element variance reduction

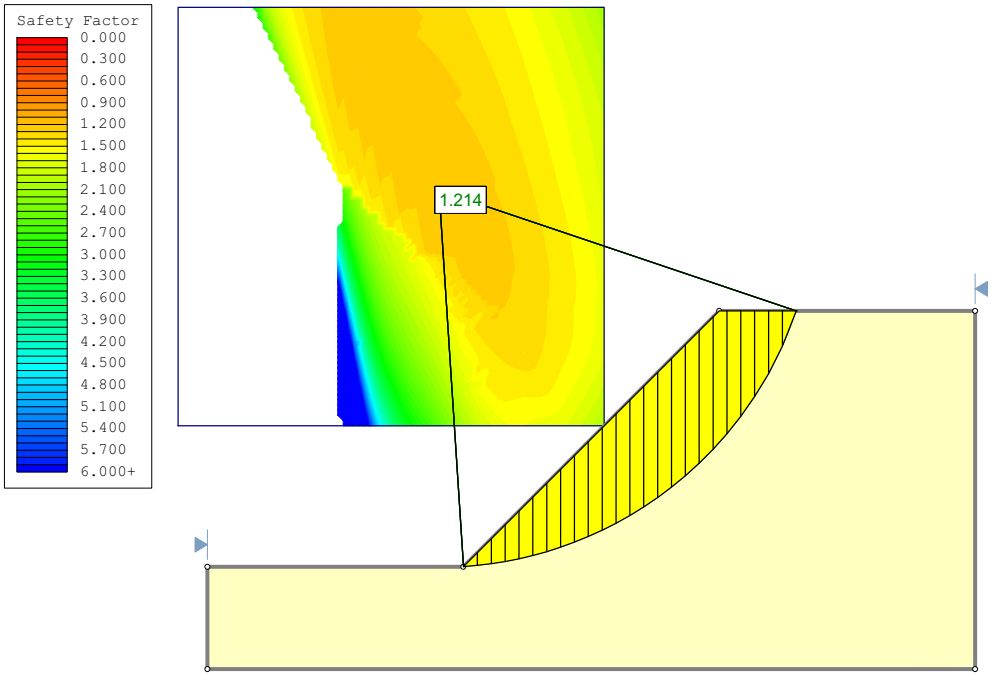

Fig. 4. Deterministic factor of safety by Spencers Method for a homogeneous c–ϕ slope from [27] using Slide by Rocscience.

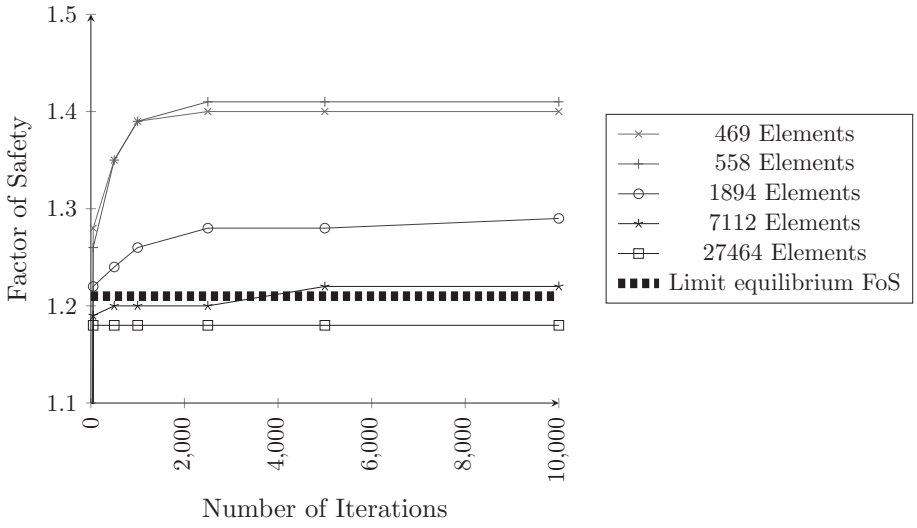

Fig. 5. Number of finite element iterations versus strength reduction factor (SRF) for different mesh refinement levels. SRF tolerance 0.01. Limit equilibrium FoS refers to the deterministic factor of safety (FoS) calculated in Section 4.3 that is to be matched to the finite element SRF.

approaches unity [14]. At high correlation lengths ($\theta_x = \theta_y$ = 1000 m and θ_x = 30 m, θ_y = 1000 m) the element variance reduction is approximately 1 for each element.

As such at these correlation lengths the error due to excessive variance reduction can be considered negligible. A histogram of the areas of each element is presented in Fig. 9.

Fig. 9 indicates that 87.6% of elements have an area less than 0.06 m^2 and 81.1% of elements have an area less than 0.05 m^2. For θ_x = 30 m, θ_y = 3 m, the effect of variance reduction is greatest. The majority of elements will, however, have their variance reduced by less than 4%. From the material property parameters given in Table 1, a 4% reduction in standard deviation will result in a 0.18 kPa in the standard deviation of cohesion and a 0.092° change in the friction angle standard deviation. The bimodality of the distribution in Fig. 9 is a result of the two levels of refinement used to grade the mesh shown in Fig. 6.

From Eq. (69), this variance reduction can be considered small enough to cause only negligible errors in the resulting analysis. The larger elements with higher variance reduction values are, from Fig. 6, positioned around the border of the mesh. These are expected to have little impact on the convergence of the finite element calculations. By using larger elements in these low impact areas, the total number of elements in the finite element mesh can be reduced, improving the time taken to carry out the probability of failure computations.

4.6. Reliability assessment

The probability of failure for the slope described in Section 4.2 was analysed with NIRFS using the finite element mesh in Fig. 6 and each of the four correlation length sets presented in Table 2. These correlation lengths were used to match those used in [27].

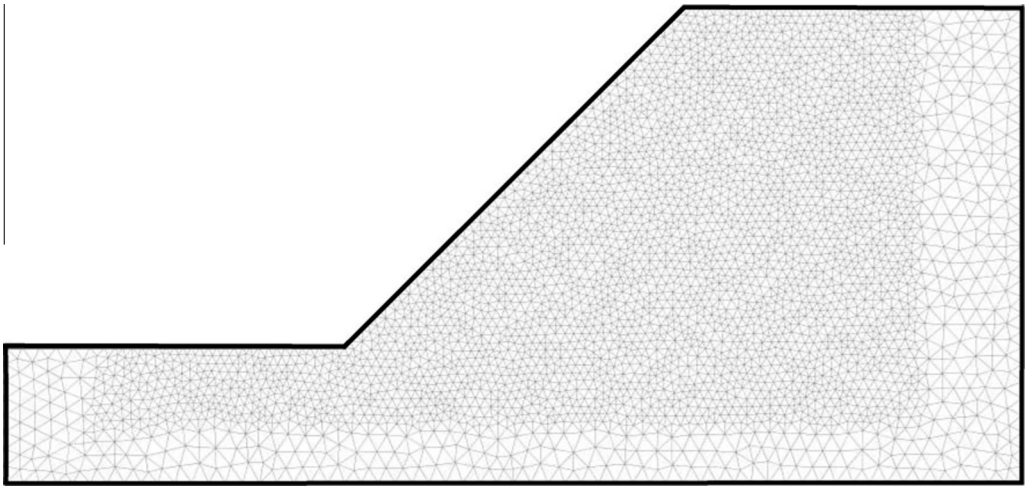

Fig. 6. Finite element mesh tested for SRF versus number of iterations with 7112 elements.

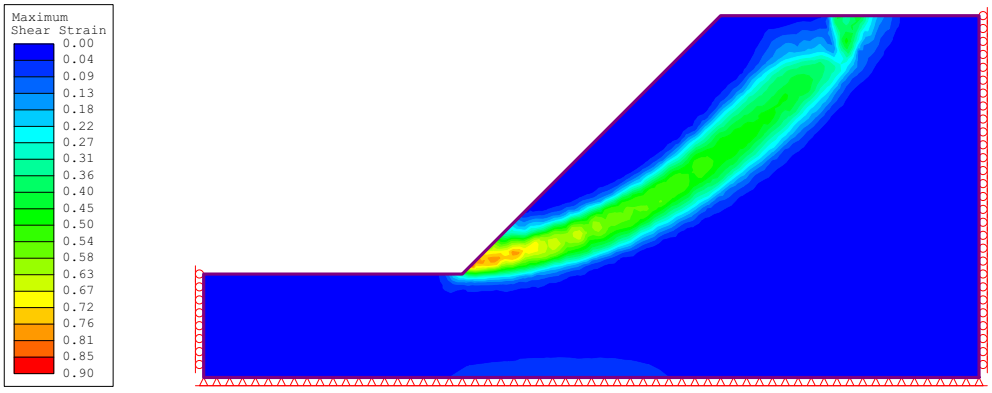

Fig. 7. Contours of maximum shear strain at critical SRF of 1.22 for finite element mesh in Fig. 6 using 5000 iterations.

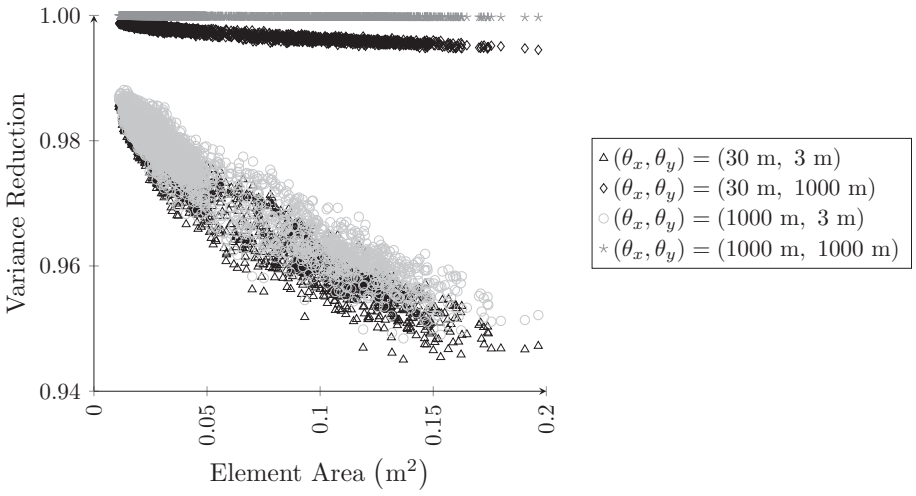

Fig. 8. Computed element variance reduction versus area for each finite element in the mesh shown in Fig. 6.

The effects of variance reduction were included in these analyses. The convergence of the probability of failure versus number of simulations is presented in Fig. 10.

After 20,000 simulations for each correlation length set, the simulation was halted. The probability of failure computed by NIRFS after 20,000 simulations is presented in Table 2.

Example outputs from NIRFS have been included to demonstrate random field sampling and discretisation. Fig. 11 presents the contours of maximum shear strain from one sample generated by NIRFS at the maximal correlation lengths tested. Fig. 12 presents an example of a failure mechanism for a discrete simulation generated by NIRFS with θ_y = 30 m and θ_y = 3 m, where

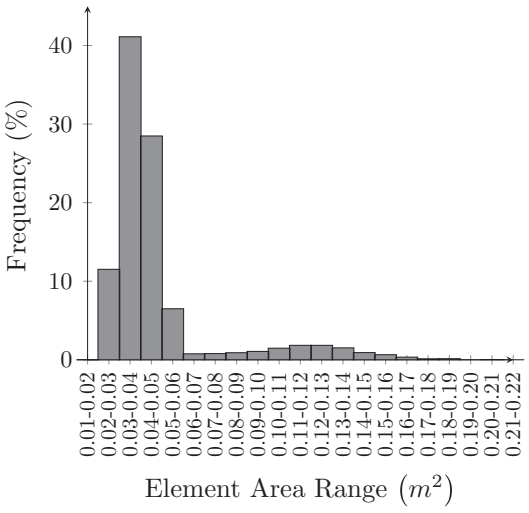

Fig. 9. Distribution of element areas for each finite element in the mesh shown in Fig. 6.

the failure mechanism is demonstrated by the contours of maximum shear strain. The friction angle and cohesion random fields used to generate Fig. 12 are shown in Figs. 13 and 14 respectively.

4.7. Discussion

The analyses demonstrate that the results computed by NIRFS are valid and conform to the trend predicted by theory presented in Mostyn and Li [32]. For a given factor of safety, changing the correlation length changes the probability of failure (as also predicted in [14]). Specifically, for slopes with factor of safety greater than one it is predicted that probability of failure increases as correlation length increases. This makes factor of safety an inconsistent measure of reliability. This discussion will consider why the computed probability of failure changes with correlation length and how this is affected by field discretisation. Additionally, the differences between the results presented in Table 2 from the authors and those computed by Ji et al. [27] are examined.

Practical aspects of field discretisation for simulation were considered. The use of local averaging allows for a random field to be discretised across an arbitrary mesh. Particularly, a graded finite element mesh can be used to reduce the total number of elements, reducing the time taken for each deterministic solution. The effect of excessive variance reduction caused by local averaging would have only a small effect on the computed probabilities of failure for the analyses presented. This was discussed in Section 4.5. The order of the variance reduction relative to the scale of the material parameters was very low even for the fairly coarse mesh used. It is noted that the mesh was constrained by the need to approximate the results in Ji et al. [27]. If the choice of mesh was less restricted standard mesh refinement techniques could be used. The effects of

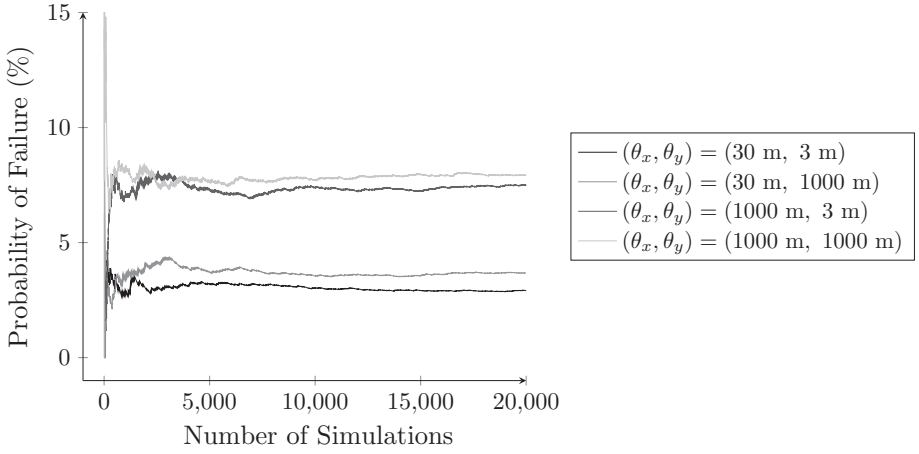

Fig. 10. Convergence of probability of failure versus number of simulations by NIRFS for the drained slope stability problem presented in Ji et al. [27].

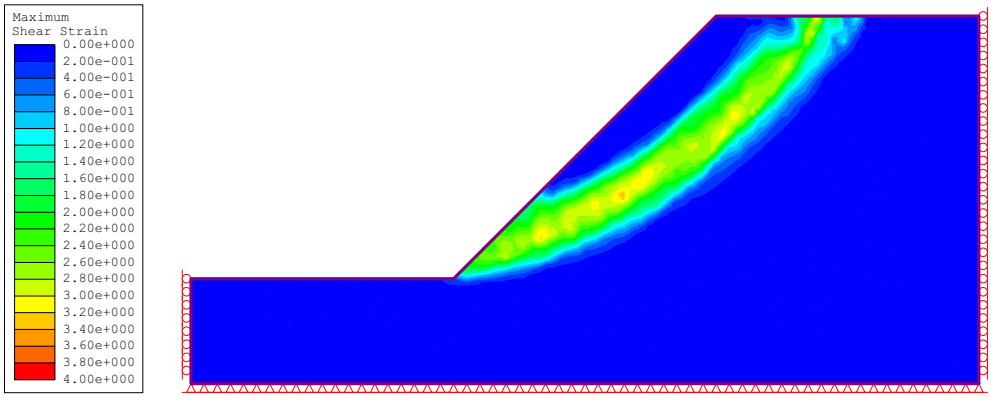

Fig. 11. Sample probabilistic failure mechanism generated by NIRFS with θ_x = 1000 m and θ_y = 1000 m. Contours show maximum shear strain.

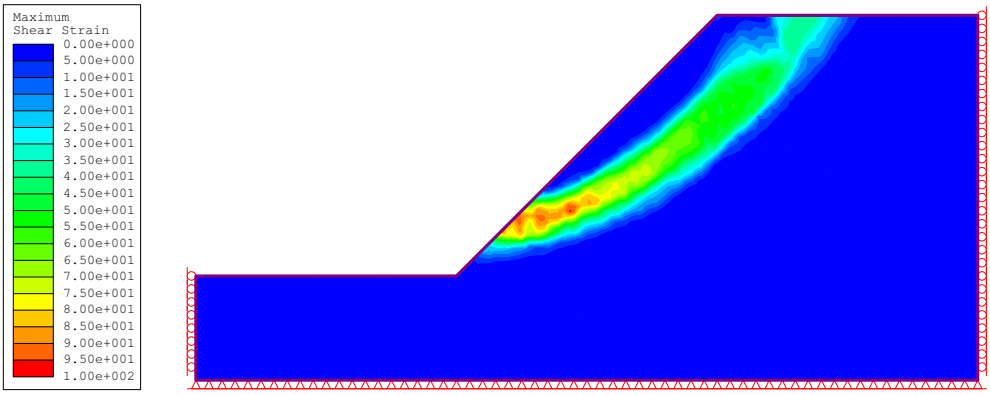

Fig. 12. Probabilistic failure mechanism generated by NIRFS with θ_x = 30 m and θ_y = 3 m. Contours show maximum shear strain.

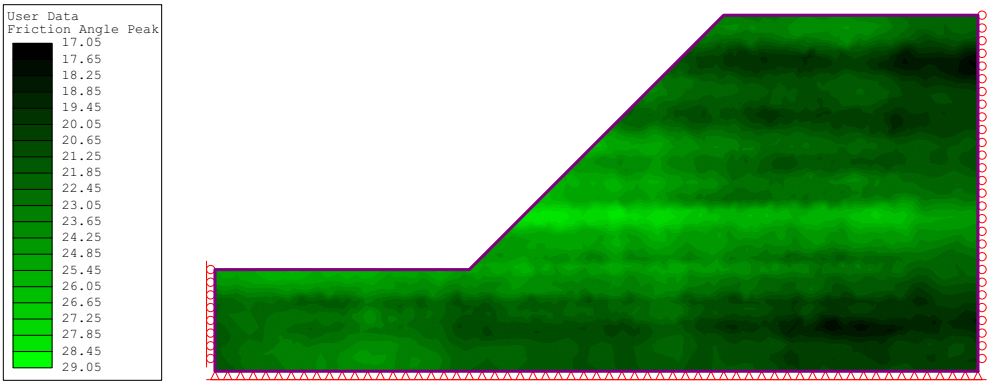

Fig. 13. Probabilistic failure mechanism generated by NIRFS with θ_x = 30 m and θ_y = 3 m. Contours show ϕ random field.

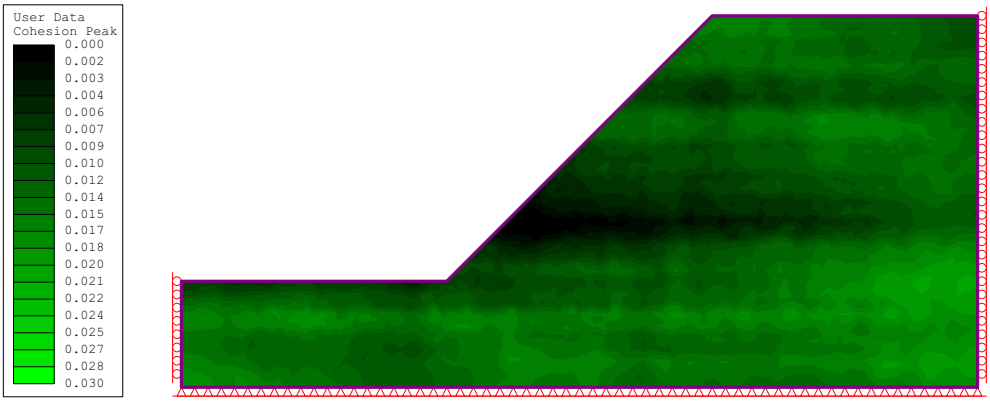

Fig. 14. Probabilistic failure mechanism generated by NIRFS with θ_x = 30 m and θ_y = 3 m. Contours show c random field.

variance reduction could then be minimised even further. Further, it is noted that the choice of correlation lengths used for the analysis are, particularly for θ_x = 30 m and θ_y = 1000 m, quite unrealistic. These lengths were used to match the analysis in [27] and were likely selected by [27] to bound the range of values for θ_x and θ_y. Measurement of correlation lengths and more realistic values are discussed in [6,21,14].

Table 2 shows that the probability of failure was observed to increase with increasing correlation length by both [27] and the authors. For the size of the problem considered, an isotropic correlation length of 1000 m is effectively infinite. In this case the variance between samples from the random field will reduce to the point variability distribution. For the slope stability problem analysed, if correlation length is infinite then each discrete RFEM simulation will be carried out with homogeneous soil shear strength. This is because c and ϕ will be constant over the soil domain. For homogeneous soil only log-spiral failure surfaces will be generated as this is the path along which the ratio of available shear resistance to failure driving forces will be lowest [17,35]. Any longer, non-logarithmic spiral failure path through the slope will be able to mobilise greater shear resistance against failure than the critical, log-spiral surface. For cases where correlation length is less than infinity, non-logarithmic spiral failure surfaces can become critical. RFEM is capable of identifying these situations as a standard part of the analysis. Also, if the correlation length is decreased from infinity the probability of sampling a homogeneous

set of soil shear strengths (low or otherwise) from the random field decreases. The probability of generating a failure in a particular discrete simulation then also decreases.

NIRFS consistently gave similar but higher probabilities than [27] except in one case. The probabilistic methods adopted by [27] analysed only the critical circular failure surface predicted by deterministic limit equilibrium. RFEM is able to investigate all possible probabilistic failure surfaces of any shape. This is the most likely cause of the different probabilities of failure computed by [27] and NIRFS shown in Table 2. As NIRFS is able to generate a more varied number of possible failure types, it can be expected that NIRFS will compute higher probabilities of failure than any limit equilibrium method that restricts failure to a single surface. Additionally, as FEM is able to generate log-spiral failure surfaces, which are more critical than circular surfaces, the probability of failure of NIRFS compared to limit equilibrium should be higher.

There was only one exception to the trend that NIRFS gave higher probabilities of failure. For isotropically infinite correlation length, NIRFS and limit equilibrium should analyse a very similar failure surface. NIRFS and limit equilibrium should then, therefore, predict a very similar probability of failure. The particularly high probability of failure computed for $\theta_x = \theta_y = 1000$ m by the method of autocorrelated slices, 17.58%, is likely some specific issue with this method. As the interpolated autocorrelation method and NIRFS computed probabilities of 7.26% and 7.92% respectively, the autocorrelated slices outlier value can be ignored. Other than a single exception, the limit equilibrium methods in [27] underestimated the probability of failure. As underestimates are, in this instance, not conservative this is a serious limitation when compared to RFEM.

5. Summary and conclusions

In this paper, a method for the mapping of random fields onto finite element meshes of arbitrarily oriented triangular elements is presented. The adopted methodology utilises a local averaging for the discretisation of the random field. Local averaging of random fields for subsequent finite element analysis helps to alleviate mesh dependence effects on probability calculations. The local averaging calculations over triangular elements presented are based on Gaussian quadrature. Earlier literature includes methods for local averaging calculations over regular quadrilateral elements. The method in this paper allows locally averaged random fields to be generated over complex geometries of the sort encountered in practice where meshes of arbitrarily oriented triangular elements are required.

The random field sampling methodology is based on Cholesky decomposition. Covariance matrices may be singular, particularly when the correlation length is large compared to the size of the finite elements. Singularity can prevent a naive Cholesky decomposition from running to completion. A technique to generate random field samples from even a singular covariance matrix is presented. Further, a priori bounds of the numerical precision of the random field samples generated by such a technique are presented. Even the very rough bounds presented indicated that the precision is sufficient for a typical RFEM analysis. If a very large number of finite elements is required, error reducing techniques such as iterative refinement may be required [23]. An iterative refinement method suitable for random field sampling would be a useful future contribution. Further, from the results in this paper it may be possible to derive a triangular mesh variant of the existing rectangular LAS in [14].

The presented random field generation methodology is then combined with the Random Finite Element Method to compute the reliability of geotechnical problems. To validate the methodology, it is compared to the results of a published reliability assessment. The results show that the methodology agrees well with theory. The method of computing the effects of local averaging over triangular elements is a special case of Gaussian quadrature over simplicial (for example tetrahedral) elements [46]. The equations for variance reduction over and covariance between tetrahedral volumes are presented in Section 2.7. Using these equations and the quadrature weights in [46], the methodology presented could be extended to mapping random field samples onto three dimensional meshes of unstructured tetrahedral elements for RFEM analysis.

References

[1] Adler RJ. The geometry of random fields (Reprint of 1980 Edition). Society for Industrial and Applied Mathematics; January 2010. http://dx.doi.org/10.1137/1.9780898718980.

[2] Ayyildiz E, Gazi VP, Wit E. A short note on resolving singularity problems in covariance matrices. Int J Stat Probab 2012;1(2):113–8. http://dx.doi.org/10.5539/ijsp.v1n2p113.

[3] Brenner SC, Carstensen C. Finite element methods. Encyclopedia of computational mechanics; November 2004. http://dx.doi.org/10.1002/0470091355.ecm003.

[4] Chang X-W, Paige CC, Stewart GW. New perturbation analyses for the Cholesky factorization. IMA J Numer Anal 1996;16(4):457–84. http://dx.doi.org/10.1093/imanum/16.4.457.

[5] Chang X-W, Stehlé D. Rigorous perturbation bounds of some matrix factorizations. SIAM J Matrix Anal Appl 2010;31(5):2841–59. http://dx.doi.org/10.1137/090778535.

[6] Cherubini C. Data and consideration on the variability of geotechnical properties of soils. Adv Saf Reliab 1997:1583–91. http://dx.doi.org/10.1016/b978-008042835-2/50178-8.

[7] Cherubini C. Probabilistic approach to the design of anchored sheet pile walls. Comput Geotech 2000;26(3–4):309–30. http://dx.doi.org/10.1016/S0266-352X(99)00044-0.

[8] Child D. The essentials of factor analysis. Bloomsbury Academic; 2006. <https://books.google.com.au/books?id=rQ2vdJgohH0C>.

[9] Cormen TH, Leiserson CE, Rivest RL, Stein C. Introduction to algorithms. The MIT Press; 2009. <http://books.google.com.au/books?id=NLngYyWFl_YC>.

[10] Cowper GR. Gaussian quadrature formulas for triangles. Int J Numer Methods Eng 1973;7(3):405–8. <http://onlinelibrary.wiley.com/doi/10.1002/nme.1620070316/abstract>.

[11] Fang H, O'Leary DP. Modified Cholesky algorithms: a catalog with new approaches. Math Program 2007;115(2):319–49. http://dx.doi.org/10.1007/s10107-007-0177-6.

[12] Farmaga I, Shmigelskyi P, Spiewak P, Ciupinski L. Evaluation of computational complexity of finite element analysis. In: CAD systems in microelectronics (CADSM), 2011 11th international conference the experience of designing and application of; February 2011. p. 213–4. <http://ieeexplore.ieee.org/xpl/login.jsp?tp=&arnumber=5744437>.

[13] Fenton GA. Error evaluation of three random field generators. J Eng Mech 1994;120(12):2478–97. http://dx.doi.org/10.1061/(ASCE)0733-9399(1994)120:12(2478).

[14] Fenton GA, Griffiths DV. Risk assessment in geotechnical engineering. John Wiley & Sons, Inc; 2008. http://dx.doi.org/10.1002/9780470284704.

[15] Fenton GA, Vanmarcke EH. Simulation of random fields via local average subdivision. J Eng Mech 1990;116(8):1733–49. http://dx.doi.org/10.1061/(asce)0733-9399(1990)116:8(1733).

[16] Friendly M, Monette G, Fox J. Elliptical insights: understanding statistical methods through elliptical geometry. Stat Sci 2013;28(1):1–39. http://dx.doi.org/10.1214/12-STS402.

[17] Garber M, Baker R. Bearing capacity by variational method. J Geotech Geoenviron Eng 1979;105(ASCE 14549 Proceeding):1209–25.

[18] Golub GH, Van Loan CF. Matrix computations. Johns Hopkins studies in the mathematical sciences. Johns Hopkins University Press; 2013. <http://books.google.com.au/books?id=X5YfsuCWpxMC>.

[19] Gray M. Modern differential geometry of curves and surfaces with mathematica. Textbooks in mathematics. Taylor & Francis; 1997. <https://books.google.com.au/books?id=-LRumtTimYgC>.

[20] Griffiths DV, Fenton GA. Probabilistic slope stability analysis by finite elements. J Geotech Geoenviron Eng 2004;130(5):507–18.

[21] Griffiths DV, Fenton GA, editors. Probabilistic methods in geotechnical engineering. CISM courses and lectures. Springer Vienna; 2007. http://dx.doi.org/10.1007/978-3-211-73366-0.

[22] Hammah RE, Yacoub TE, Curran JH, Corkum BC. The shear strength reduction method for the generalized Hoek-Brown criterion. In: Alaska Rocks 2005, the 40th US symposium on rock mechanics (USRMS); 2005. <http://www.onepetro.org/mslib/servlet/onepetropreview?id=ARMA-05-810>.

[23] Higham NJ. Accuracy and stability of numerical algorithms; January 2002. http://dx.doi.org/10.1137/1.9780898718027.

[24] Horn RA, Johnson CR. Matrix analysis. Cambridge University Press; 2012. <https://books.google.com.au/books?id=5I5AYeeh0JUC>.

[25] Huang YH. Slope stability analysis by the limit equilibrium method. American Society of Civil Engineers; 2014. http://dx.doi.org/10.1061/9780784412886.
[26] IEEE. IEEE standard for floating-point arithmetic. IEEE Std 754-2008; August 2008. p. 1–70. http://dx.doi.org/10.1109/IEEESTD.2008.4610935.
[27] Ji J, Liao HJ, Low BK. Modeling 2-D spatial variation in slope reliability analysis using interpolated autocorrelations. Comput Geotech 2012;40:135–46. http://dx.doi.org/10.1016/j.compgeo.2011.11.002.
[28] Kaggwa GWS, Kuo YL. Probabilistic techniques in geotechnical modelling-which one should you use? Aust Geomech 2011;3(46):21–8. <http://hdl.handle.net/2440/71912>.
[29] Kroese DP, Chan JCC. Statistical modeling and computation; 2014. http://dx.doi.org/10.1007/978-1-4614-8775-3.
[30] Marks E. A note on a geometric interpretation of the correlation coefficient. J Educ Stat 1982;7(3):233. http://dx.doi.org/10.2307/1164647.
[31] Meyer C. Matrix analysis and applied linear algebra. SIAM; 2000. http://dx.doi.org/10.1137/1.9780898719512.
[32] Mostyn GR, Li KS. Probabilistic slope analysis – state of play. In: Proceedings of the conference on probabilistic methods in geotechnical engineering. Rotterdam: Balkema; 1993. p. 89–109.
[33] Mostyn GR, Soo S. The effect of autocorrelation on the probability of failure of slopes. In: 6th Australia, New Zealand conference on geomechanics: geotechnical risk; 1992. p. 542–6.
[34] Papaioannou I, Straub D. Reliability updating in geotechnical engineering including spatial variability of soil. Comput Geotech 2012;42:44–51. <http://www.sciencedirect.com/science/article/pii/S0266352X11001984>.
[35] Puła O, Puła W, Wolny A. On the variational solution of a limiting equilibrium problem involving an anchored wall. Comput Geotech 2005;32(2):107–21. http://dx.doi.org/10.1016/j.compgeo.2005.01.002.
[36] Puła W. On some aspects of reliability computations in bearing capacity of shallow foundations. Probab Methods Geotech Eng 2007:127–45. http://dx.doi.org/10.1007/978-3-211-73366-0_5.
[37] Schmid J. The relationship between the coefficient of correlation and the angle included between regression lines. J Educ Res 1947;41(4):311–3. http://dx.doi.org/10.1080/00220671.1947.10881608.
[38] Stefanou G. The stochastic finite element method: past, present and future. Comput Methods Appl Mech Eng 2009;198(9–12):1031–51. <http://www.sciencedirect.com/science/article/pii/S0045782508004118>.
[39] Strang G, Fix G. An analysis of the finite element method. Prentice-Hall series in automatic computation. Wellesley-Cambridge Press; 2008. <https://books.google.com.au/books?id=K5MAOwAACAAJ>.
[40] Sudret B, Der Kiureghian A. Stochastic finite element methods and reliability: a state-of-the-art report. Department of Civil and Environmental Engineering, University of California; 2000.
[41] Szynakiewicz T, Griffiths DV, Fenton GA. A probabilistic investigation of c-phi'slope stability. Proceedings of the 6th international congress on numerical methods in engineering and scientific applications, vol. 2536. Caracas: Sociedad Venezolana de Metodos Numericos en Ingenieria; 2002.
[42] Trangenstein JA. Numerical solution of elliptic and parabolic partial differential equations. Cambridge University Press; 2013. http://dx.doi.org/10.1017/CBO9781139025508.
[43] Vanmarcke E. Random fields: analysis and synthesis. 2nd ed. World Scientific; 2010. http://dx.doi.org/10.1142/5807.
[44] Vanmarcke E, Shinozuka M, Nakagiri S, Schuëller G, Grigoriu M. Random fields and stochastic finite elements. Struct Saf 1986;3(3–4):143–66. http://dx.doi.org/10.1016/0167-4730(86)90002-0.
[45] Vořechovskỳ M, Novák D. Simulation of random fields for stochastic finite element analyses. In: Proc 9th international conference on structural safety and reliability (ICOSSAR'05), vol. 5; 2005. p. 2545–52. <http://www.fce.vutbr.cz/stm/vorechovsky.m/papers/18z.pdf>.
[46] Walkington N. Quadrature on simplices of arbitrary dimension. Carnegie Mellon University, Department of Mathematical Sciences, Center for Nonlinear Analysis; 2000. <http://www.math.cmu.edu/nw0z/publications/00-CNA-023/>.
[47] Yiu P. The uses of homogeneous barycentric coordinates in plane euclidean geometry. Int J Math Educ Sci Technol 2000;31(4):569–78. <http://www.tandfonline.com/doi/abs/10.1080/002073900412679>.